Cationic Zirconocene Olefin Polymerization Catalysts Based on the Organo-Lewis Acid Tris(pentafluorophenyl)borane. A Synthetic, Structural, Solution Dynamic, and Polymerization Catalytic Study

Xinmin Yang, Charlotte L. Stern, and Tobin J. Marks*

Contribution from the Department of Chemistry, Northwestwern University, Evanston, Illinois 60208-3113

Received April 13, 1994®

Abstract: The reaction of $B(C_6F_5)_3$ with zirconocene dimethyl complexes L_2ZrMe_2 in hydrocarbon solvents affords base-free cationic zirconium complexes $L_2ZrMe^+MeB(C_6F_5)_3^-$ (L = η^5-C_5H_5, **1**; η^5-$Me_2C_5H_3$, **2**; η^5-Me_5C_5, **3**; η^5-$(TMS)_2C_5H_3$, **4**) in quantitative yields. A similar reaction using $(^tBu_2C_5H_3)_2ZrMe_2$ results in the formation of the cationic metallacyclic product $(^tBu_2C_5H_3)[^tBuC_5H_3C(Me_2)CH_2]Zr^+MeB(C_6F_5)_3^-$ (**6**) through what is presumably an intramolecular C–H activation process. Complexes **3** and **6** undergo rapid hydrogenolysis to yield the corresponding cationic hydrido complexes $(Me_5C_5)_2ZrH^+MeB(C_6F_5)_3^-$ (**7**), $(Me_5C_5)_2ZrH^+HB(C_6F_5)_3^-$ (**8**) (stepwise), and $(^tBu_2C_5H_3)_2ZrH^+MeB(C_6F_5)_3^-$ (**9**), respectively. Complex **2** undergoes slow conversion to $\{[(Me_2C_5H_3)_2ZrMe]_2(\mu\text{-}F)\}^+MeB(C_6F_5)_3^-$ (**12**) in C_6D_6 under an inert atmosphere at 25 °C. Complexes **2**, **3**, **4**, **6**, **8**, and **12** have been characterized by X-ray diffraction (crystal data: **2**, monoclinic, $P2_1/n$, a = 12.261(2) Å, b = 20.010(6) Å, c = 13.053(5) Å, β = 90.80(2)°, R = 0.027; **3**, monoclinic, $P2_1/n$, a = 9.405(1) Å, b = 19.336(3) Å, c = 10.382(1) Å, β = 96.54(1)°, R = 0.039; **4**, triclinic, $P\bar{1}$, a = 11.639(4) Å, b = 12.877(4) Å, c = 19.224(4) Å, α = 77.89(2)°, β = 74.33(2)°, γ = 77.04(3)°, R = 0.043; **6**, monoclinic, $P2_1$, a = 12.610(5) Å, b = 20.995(4) Å, c = 21.389(5) Å, β = 106.13(3)°, R = 0.066; **8**, triclinic, $P\bar{1}$, a = 11.899(4) Å, b = 12.643(4) Å, c = 13.681(4) Å, α = 84.47(2)°, β = 76.12(3)°, γ = 65.34(3)°, R = 0.060; **12**, triclinic, P_1, a = 12.308(1) Å, b = 13.898(3) Å, c = 15.182(2) Å, α = 101.63(1)°, β = 90.42(1)°, γ = 115.22(1)°, R = 0.031). These structure determinations allow detailed analysis of the metrical aspects of $L_2ZrMe^+MeB(C_6F_5)_3^-$ ion pairing on the solid state. As revealed by dynamic ^1H NMR, complexes **1–4** undergo rapid intramolecular Zr–Me/B–Me exchange ($\Delta G^‡(\sigma$, kcal/mol, °C, complex) = 18.7(2, 80, **1**); 19.7(2, 80, **2**); 19.8(2, 80, **3**); 18.0(2, 35, **4**)) and for **2** and **4**, symmetrizing ion-pair dissociation–recombination processes ($\Delta G^‡(\sigma$, kcal/mol, °C, complex) = 18.3(2, 80, **2**); 14.4(2, 35, **4**)). Complexes **1–4**, **7**, and **8** are highly active homogeneous catalysts for the polymerization of ethylene with activities (3.2–6.8 × 10^6g polyethylene/mol Zr h atm at 25 °C) comparable to methylalumoxane-based zirconocene catalysts. Complexes **1–3**, **7** and **8** are also active for the atactic polymerization of propylene. In regard to polymerization chain transfer mechanisms, NMR endgroup analysis and labeling experiments using $CH_2{=}CH^{13}CH_3$ indicate the predominant pathway for **1** and **2** is β-H elimination, while for **3** it is β-CH_3 elimination. These experiments unambiguously rule out propylene C–H activation processes as an important chain transfer pathway. Complex **9** is highly active for the catalytic dimerization of propylene (N_t = 0.25 s^{-1} at 20 °C) to form a mixture of 2-methyl-1-pentene and 2-methyl-2-pentene.

Introduction

Agents for single-site, homogeneous group 4 metallocene-based olefin polymerization are currently of great scientific and technological interest in catalysis and polymer chemistry.[1,2] Compared to traditional Ziegler–Natta catalysts, the active site homogeneity and the tailorability of this new generation of catalysts offers unprecedented control over the properties of the polymeric products. To form active catalysts, group 4 metallocenes must be activated by Lewis acidic cocatalysts such as methylalumoxane (MAO),[2,3] alkylaluminum halides,[4] or dehydroxylated alumina (DA) and related oxides.[5] Although many of its constitutional features remain unclear, MAO is currently by far the most effective metallocene cocatalyst, and MAO-containing catalyst systems have therefore been the most widely studied. The role of these cocatalysts is now generally thought to be facilitating the formation of electron-deficient/coordinatively

* Abstract published in *Advance ACS Abstracts*, September 1, 1994.

(1) For recent reviews of olefin polymerization catalysts, see: (a) *Transition Metal Catalyzed Polymerizations*; Quirk, R. P., Ed.; Cambridge University Press: Cambridge, **1988**. (b) *Transition Metals and Organometallics for Catalysts for Olefin Polymerization*; Kaminsky, W., Sinn, H., Ed.; Springer: New York, 1988. (c) *Catalytic Polymerization of Olefins*; Keii, T., Soga, K., Eds.; Elsevier: Amsterdam, 1986. (d) Pino, P.; Rötzinger, B. *Makromol. Chem. Phys. Suppl.* **1984**, *7*, 41–61. (e) *Transition Metal Catalyzed Polymerization. Alkenes and Dienes*; Quirk, R. P., Hsieh, H. L., Klingensmith, G. C., Tait, P. J., Eds.; Harwood Publishers for MMI Press: New York, 1983. (f) Boor, J. *Ziegler–Natta Catalysts and Olefin Polymerization*: Academic Press: New York, 1979.

(2) For some recent references, see: (a) Erker, G.; Aulbach, M.; Kruger, C.; Werner, S. *J. Organomet. Chem.* **1993**, *450*, 1–7. (b) Farina, M.; Disilvestro, G.; Sozzzni, P. *Macromolecules* **1993**, *26*, 946–950. (c) Girdello, M. A.; Eisen, M. S.; Stern, C. L.; Marks, T. J. *J. Am. Chem. Soc.* **1993**, *115*, 3326–3327. (d) Siedle, A. R.; Lamanna, W. M.; Olofson, J. M.; Nerad, B. A.; Newmark, R. A. *ACS Symp. Ser.* **1993**, *517*, 156–167. (e) Kaminsky, W.; Bark, A.; Steiger, R. *J. Mol. Cat.* **1992**, *74*, 109–119. (f) Chien, J. C. W.; Llinas, G. H.; Rausch, M. D.; Lin, Y. G.; Winter, H. H.; Atwood, J. L.; Bott, S. G. *J. Poly. Sci. Part A. Poly. Chem.* **1992**, *30*, 2601–2617. (g) Okuda, J. *Angew. Chem., Int. Ed. Engl.* **1992**, *31*, 47–48. (h) Leaversuch, R. D. *Modern Plastics* **1991**, 46–49. (i) Resconi, L.; Abis, L.; Franciscono, G. *Macromolecules* **1992**, *25*, 6814–6817. (j) Waymouth, R.; Pino, P. *J. Am. Chem. Soc.* **1990**, *112*, 4911–4914. (k) Ewen, J. A.; Jones, R. L.; Razavi, A.; Ferrara, J. D. *J. Am. Chem. Soc.* **1988**, *110*, 6255–6256.

(3) (a) Kaminsky, W. Kulper, K.; Brintzinger, H. *Angew. Chem., Int. Ed. Engl.* **1985**, *24*, 507–509. (b) Ginantti, E.; Nicoletti, G. M.; Mazzocchi, R. *J. Poly. Sci: Poly Chem. Ed.* **1985**, *23*, 2117–2133. (c) Ewen, J. A. *J. Am. Chem.Soc.* **1984**, *106*, 6355–6264. (d) Herwig, J.; Kaminsky, W. *Polymer Bull.* **1983**, *9*, 417. (e) Kaminsky, W.; Miri, M.; Sinn, H.; Woldt, R. *Macromol. Chem. Rapid Commun.* **1983**, *4*, 417–421. (f) Sinn, H.; Kaminsky, W. *Adv. Organomet. Chem.* **1980**, *18*, 99–149.

(4) (a) Long, W. P.; Breslow, D. S. *J. Am. Chem. Soc.* **1960**, *82*, 1953–1957. (b) Breslow, D. S.; Newburg, N. R. *J. Am.Chem. Soc.* **1957**, *79*, 5072.

(5) (a) Marks, T. J. *Acc. Chem. Res.* **1992**, *25*, 57–65 and reference therein. (b) Dahmen, K–H.; Hedden, D.; Burwell, R. L., Jr.; Marks, T. J. *Langmuir* **1988**, *4*, 1212–1214.

0002-7863/94/1516-10015$04.50/0

unsaturated "cationic" metallocene alkyl species (I, eq 1), which

$$Cp_2M\begin{matrix}R\\R'\end{matrix} + A \rightleftharpoons Cp_2\overset{+}{M}\begin{matrix}R\\ \end{matrix}\ R'\text{-}A^- \quad (1)$$

I

are the actual catalysts (Cp = cyclopendadienyl-type ligand; M = Ti, Zr, Hf; R = alkyl; R′ = alkyl or halide; A = cocatalyst). Originally proposed on the basis of early UV–visible spectroscopic[4] and electrodialysis experiments,[6] the scenario of eq 1 is further supported by evidence from more recent chemical trapping,[7] XPS,[8] solution,[9] and solid state[5b,10] NMR spectroscopic studies. Further evidence derives from the observation of polymerization activity in a variety of specially designed model complexes with structures generally analogous to I[11,12] and in isoelectronic, neutral organonolanthanide[13,14] and organoscandium[15] complexes.

It is clear that MAO has a very complicated and often variable composition and structurally remains incompletely characterized.[16] It has not been possible to isolate characterizable metallocene active species using either MAO, aluminum alkyls, or DA as cocatalysts. Detailed structural information about the active species formed in such systems, which is crucial in the understanding of polymerization activities, stereoregulation, and chain transfer/termination processes, is not likely to be obtained. Thus, unambiguous demonstration of the putative metallocene–cocatalyst interaction as illustrated in eq (1) is presently an incompletely realized goal.

Our strategy to address this problem is based on the hypothesis that if the role of the cocatalysts is indeed what has been proposed in eq 1, then it might be possible to devise other potent Lewis acids which are as effective as cocatalysts but which can form *isolable* and *characterizable* catalysts with group 4 metallocenes. We chose the simple organoborane $B(C_6F_5)_3$[17] for three reasons. Firstly, it is a relatively strong molecular Lewis acid (acidity between BCl_3 and BF_3) and has been shown to form a variety of characterizable Lewis base adducts. Secondly, it has good solubility in nonpolar, noncoordinating solvents. Thirdly, the boron center is surrounded by highly electronegative, chemically robust (i.e., resistant to electrophilic attack) functional groups having only nonpolar, minimally coordinating fluoro substituents. Using this borane we have been able to isolate a variety of cationic zirconocene alkyl and hydrido complexes which are highly active catalysts for the polymerization of ethylene and α-olefins. A large body of precise diffraction structural information has also been obtained. We report here results of a detailed study of the synthesis, solid state structures, spectroscopic, solution dynamic, and catalytic properties of a series of such complexes.[18]

Experimental Section

Materials and Methods. All operations were performed with rigorous exclusion of oxygen and moisture in flamed Schlenk-type glassware on a dual-manifold Schlenk line or interfaced to a high-vacuum line (10^{-5} Torr) or in a dinitrogen-filled, Vacuum Atmospheres glovebox with a high capacity atmosphere recirculator (1–2 ppm O_2). Argon (Matheson, prepurified), ethylene (Matheson, CP), propylene (Matheson, PP), and propylene (3-^{13}C, 99%, Merck Sharp Dohme Isotopes, Canada) were additionally purified by passage through a supported MnO oxygen-removal column and a Davison 4Å molecular sieve column. Hydrocarbon solvents (toluene, pentane) were distilled under nitrogen from Na/K alloy. Ether solvents (THF, Et_2O) were distilled under nitrogen from sodium benzophenone ketyl. All solvents were stored in vacuo over Na/K in Teflon-valved bulbs. Deuterated solvents were from Cambridge Isotope Laboratories (all ≥99 atom % D) and were degassed and dried over Na/K alloy and stored in resealable flasks. BrC_6F_5 (Aldrich) was dried over molecular sieves. BCl_3 (in hexane) and ^{n}BuLi (1.6 M in hexane) (Aldrich) were used as received.

The zirconocene complexes $Cp_2Zr(CH_3)_2$,[19a] $Cp_2Zr(CH_3)Cl$,[19b], $(1,2\text{-}Me_2C_5H_3)_2Zr(CH_3)_2$[20] ($Cp_2''Zr(CH_3)_2$), $(C_5Me_5)_2Zr(CH_3)_2$,[21] ($Cp_2'Zr(CH_3)_2$), $[1,3\text{-}(SiMe_3)_2C_5H_3]_2ZrCl_2$,[22] $(1,3\text{-}^tBu_2C_5H_3)_2ZrCl_2$,[23] $(C_5Me_5)_2ZrH_2$,[21,24] ($Cp_2'ZrH_2$), $Cp_2Zr(CH_2Ph)_2$,[25] and $Cp_2Zr(CH_3)CH_2Ph$[26] were prepared according to literature procedures. The reagent $B(C_6F_5)_3$ was prepared by the method of Massey and Park[17] and was purified by repeated vacuum sublimation. BPh_3 was purchased from Aldrich.

Physical and Analytical Measurements. NMR spectra were recorded on a Varian XL-400 (FT, 400 MHz, ^{1}H; 100 MHz, ^{13}C; 376 MHz, ^{19}F; 128 MHz, ^{11}B) or a Varian Germini-300 (FT 300 MHz, ^{1}H; 75 MHz, ^{13}C; 282 MHz, ^{19}F) spectrometer. Chemical shifts for ^{1}H and ^{13}C spectra were referenced using internal solvent resonances and are reported relative to tetramethylsilane. ^{19}F NMR spectra were referenced to external $CFCl_3$. ^{11}B NMR was referenced to external $Et_2O{\cdot}BF_3$. NMR spectroscopic experiments on air-sensitive samples were conducted in Teflon valve-sealed sample tubes (J. Young). Elemental analyses were performed by Oneida Research Services, Inc., Whitesboro, New York. GPC analysis of polymer samples was performed at Akzo Chemical Co.

(6) D'yachkovskii, F. S.; Shilova, A. K.; Shilov, A. Y. *J. Polym. Sci. C* **1967**, 2333–2339.
(7) Eisch, J. J.; Piotrowski, A. M.; Brownstein, S. K.; Gabe, E.; J.; Lee, F. L. *J. Am. Chem. Soc.* **1985**, *107*, 7219–7200.
(8) Gassman, P. G.; Callstrom, M. R. *J. Am. Chem. Soc.* **1987**, *109*, 7875–7876.
(9) (a) Tritto, I.; Li, S.; Sacchi, M. C.; Zannoni, G. *Macromolecules* **1993**, *26*, 7111–7115 and references therein. (b) Eisch, J. J.; Caldwell, K. R.; Werner, S.; Kruger, K. *Organometallics* **1991**, *10*, 3417–3419. (c) Resconi, L.; Bossi, S.; Abis, L. *Macromolecules* **1990**, *23*, 4489–4491.
(10) Sishta, C.; Hathorn, R.; Marks, T. J. *J. Am. Chem. Soc.* **1992**, *114*, 1112–1114.
(11) For recent reviews, see: ref 5a and Jordan, R. F. *Adv. Organomet. Chem.* **1991**, *32*, 325–387, and reference therein.
(12) For other important references not covered by the above reviews, see: (a) Borkowsky, S. L.; Baenziger, N. C.; Jordan, R. F. *Organometallics* **1993**, *12*, 486–495. (b) Alelynnas, Y. W.; Guo, Z.; La Pointe, R. E.; Jordan, R. F. *Organometallics* **1993**, *12*, 544–553. (c) Bochmann, M.; Lancaster, S. J. *Organometallics* **1993**, *12*, 633–640, and references therein. (d) Bochmann, M.; Jaggar, A. J. *J. Organomet. Chem.* **1992**, *434*, C1–C5. (e) Horton, A. D.; Oppen, A. G. *Organometallics* **1992**, *11*, 8–10. (f) Horton, A. D.; Orpen, A. G. *Organometallics* **1991** *10*, 3910–3918. (g) Eshuis, J. J.; Tan, Y. Y.; Meetsma, A.; Teuben, J. H. *Organometallics* **1992**, *11*, 362–369 and references therein. (h) Chien, J. C. W.; Tsai, W. M.; Rausch, M. D. *J. Am. Chem. Soc.* **1991**, *113*, 8570–8571. (i) Amorose, D. M.; Lee, R. A.; Petersen, J. L. *Organometallics* **1991**, *10*, 2191–2198. (j) Hlatky, G. G.; Turner, H. W.; Eckman, R. R. *J. Am. Chem. Soc.* **1989**, *111*, 2728–2729. (k) Haltky, G. G.; Eckman, R. R.; Turner, H. W. *Organometallics* **1992**, *11*, 1413–1416. (l) Taube, R.; Krukowa, L. *J. Organomet. Chem.* **1988**, *347*, C9–C11.
(13) (a) Watson, P. L.; Parshall, W. *Acc. Chem. Res.* **1985**, *18*, 51–56, and references therein. (b) Similar reaction patterns are observed for organothorium metallacycles: Fendrick, C. M.; Marks, T. J. *J. Am. Chem. Soc.* **1986**, *108*, 425–437.
(14) Jeske, G.; Lauke, H.; Mauermann, H.; Sweptson, P. N.; Schumann, H.; Marks, T. J. *J. Am. Chem. Soc.* **1985**, *107*, 8091–8103, 8111–8118.
(15) (a) Bunel, E.; Burger, B. J.; Bercaw, J. E. *J. Am. Chem. Soc.* **1988**, *110*, 976–978. (b) Burger, B. J.; Thompson, M.; Cotter, D.; Bercaw, J. E. *J. Am. Chem. Soc.* **1990**, *122*, 1566–1577. (c) Shapiro, P. J.; Cotter, W. D.; Schaefer, W. P.; Labinger, J. A.; Bercaw, J. E. *J. Am. Chem. Soc.* **1994**, *116*, 4623–4640.
(16) (a) Mason, M. R.; Smith, J. M.; Bott, S. G.; Barron, A. R. *J. Am. Chem. Soc.* **1993**, *115*, 4971–4984, and references therein. (b) Sugano, T.; Matsubara, K.; Fugita, T.; Takahashi, T. *J. Mol. Catal.* **1993**, *82*, 93–101.
(17) (a) Massey, A. G.; Park, A. J. *J. Oranomet. Chem.* **1964**, *2*, 245–250. (b) Massey, A. G.; Park, A. J. *J. Organomet. Chem.*, **1966**, *5*. 218–225.
(18) (a) Several weeks subsequent to the publication of our initial communication on this subject,[18b] a European Patent Application[18c] appeared teaching the use of zirconocenes + aluminum alkyls + Lewis acids as α-olefin polymerization catalysts. The preferred Lewis acids used in combination with aluminum alkyls contain boron or $MgCl_2$, with $B(C_6F_5)_3$ most preferred. (b) Yang, X.; Stern, C. L.; Marks, T. J. *J. Am. Chem. Soc.* **1991**, *113*, 3623–3625. (c) Ewen, J. A.; Edler, M. J. *CA-A* **1991**, 2, 027, 145; *Chem. Abstr.* **1991**, *115*, 136998g, 256895t.
(19) (a) Samuel, E.; Rausch, M. D. *J. Am. Chem. Soc.* **1973**, *95*, 6263. (b) Wailes, P. C.; Weigold, H.; Bell, A. P. *J. Organomet. Chem.* **1972**, *34*, 155–165.
(20) Smith, G. M., Ph.D. Thesis, Northwestern University, 1985.
(21) Manriquez, J. M.; McAlister, D. R.; Sanner, R. D.; Bercaw, J. E. *J. Am. Chem. Soc.* **1978**, *100*, 2716–2724.
(22) Antinolo, A.; Lappert, M. F.; Singh, A.; Winterborn, D. J. W.; Engelhardt, L. M.; Raston, C. L.; White, A. H.; Carty, A.; Taylor, N. J. *J. Chem. Soc., Dalton Trans.* **1987**, 1643–1472.
(23) Urazowski, I. F.; Donomaryev, V. I.; Nifant'ev, I. E.; Lemenovskii, D. A. *J. Organomet. Chem.* **1989**, *368*, 287–294.
(24) Schock, L. E.; Brock, C. P.; Marks, T. *J. Am. Chem. Soc.* **1988**, *110*, 7701–7715.
(25) Fachinetti, G.; Fochi, G.; Floriani, C. *J. Chem. Soc., Dalton Trans.* **1977**, 1946–1950.
(26) Brindley, P. B.; Scotton, M. J. *J. Chem. Soc., Perkin Trans. II* **1981**, 419–423.

$Cp_2ZrCH_3^+CH_3B(C_6F_5)_3^-$ (1). Cp_2ZrMe_2 (0.100 g, 0.398 mmol) and $B(C_6F_5)_3$ (0.205 g, 0.400 mmol) were charged into a 25-mL reaction flask in the glovebox. On the vacuum line, benzene (15 mL) was then vacuum-transferred into this flask at −78 °C. The mixture was slowly warmed to room temperature and stirred for 1.5 h. Large quantities of solid were observed to precipitate. Pentane (10 mL) was next vacuum-transferred into the flask, and the mixture was filtered after stirring. The light yellow solid which collected was washed once with 5 mL of pentane and dried under vacuum: yield 72%. Anal. Calcd for $C_{30}H_{16}BF_{15}Zr$: C, 47.20; H, 1.90; N, 0.00. Found: C, 46.98; H, 1.90; N, 0.00.

$Cp''_2ZrCH_3^+CH_3B(C_6F_5)_3^-$ (2). Cp''_2ZrMe_2 (0.116 g, 0.378 mmol) and $B(C_6F_5)_3$ (0.194 g, 0.379 mmol) were loaded into a 25-mL flask. Benzene (10 mL) was then vacuum transferred into this flask at −78 °C. The mixture was slowly warmed to ambient temperature. A clear solution was observed initially, but it quickly became cloudy as solids began to precipitate. After stirring for 2.5 h, the mixture was filtered. The light yellow solid which collected was washed once with a small amount of benzene and dried under vacuum: yield 65%. Anal. Calcd for $C_{34}H_{24}BF_{15}Zr$: C, 49.83; H, 2.95; N, 0.00. Found: C, 49.69; H, 2.83; N, 0.02.

$Cp'_2ZrCH_3^+CH_3B(C_6F_5)_3^-$ (3). The title complex was synthesized using the same procedure as for **1** by reacting Cp'_2ZrMe_2 (0.17 g, 0.435 mmol) and $B(C_6F_5)_3$ (0.250 g, 0.488 mmol) in 15 mL of benzene: yield 82%; ^{11}B NMR (C_6D_6 + THF-d_8, 25 °C) δ −14.01. Anal. Calcd for $C_{40}H_{36}BF_{15}Zr$: C, 53.16; H, 4.01; N, 0.00. Found, C, 53.07; H, 3.87; N, 0.00.

$[1,3\text{-}(SiMe_3)_2C_5H_3]_2ZrCH_3^+CH_3B(C_6F_5)_3^-$ (4). The title complex was synthesized using the same procedure as for **2** by reacting $[1,3\text{-}(SiMe_3)_2C_5H_3]_2Zr(CH_3)_2$ (0.40 g, 0.690 mmol, synthesized by the reaction of $[1,3\text{-}(SiMe_3)_2C_5H_3]_2ZrCl_2$ with excess of MeLi in a toluene) and $B(C_6F_5)_3$ (0.40 g, 0.780 mmol) in 20 mL of pentane: yield 80%. Anal. Calcd for $C_{42}H_{48}BSi_4F_{15}Zr$: C, 47.94; H, 4.60. Found: C, 47.82; H, 4.48.

$[1,3\text{-}(CMe_3)_2C_5H_3][CMe_3C_5H_3C(Me_2)CH_2]Zr^+MeB(C_6F_5)_3^-$ (6). $[1,3\text{-}(CMe_3)_2C_5H_3]_2ZrMe_2$ (0.21 g, 0.442 mmol) and $B(C_6F_5)_3$ (0.21 g, 0.410 mmol) were reacted in 15 mL of toluene at room temperature for 10 h. The solution was filtered and cooled to −78 °C. The product which precipitated out was collected by filtration and dried under vacuum: yield 67%. Anal. Calcd for $C_{47}H_{44}BF_{15}Zr$: C, 55.62; H, 4.56. Found: C, 55.61; H, 4.52.

$Cp'_2ZrH^+MeB(C_6F_5)^-$ (7). $Cp'_2Zr(CH_3)_2$ (82 mg, 0.210 mmol) and $B(C_6F_5)_3$ (123 mg, 0.240 mmol) were loaded into a 25-mL reaction flask. Pentane (15 mL) was condensed in at −78 °C. The flask was then backfilled with 1 atm of H_2. The suspension was stirred at −78 °C for 2 h and then at 25 °C for 15 h. It was next filtered, and the resulting light yellow solid was collected by filtration, washed with 10 mL of pentane, and dried under vacuum: yield 80%. Anal. Calcd for $C_{39}H_{34}BF_{15}Zr$: C, 52.65; H, 3.85. Found: C, 52.75; H, 3.59.

$Cp'_2ZrH^+HB(C_6F_5)_3^-$ (8). Procedure A: similar to that of **1**, except the reaction was carried out in benzene. Procedure B: Cp'_2ZrH_2 (150 mg, 0.413 mmol) and $B(C_6F_5)_3$ (230 mg, 0.449 mmol) were reacted in 15 mL of toluene in a 25-mL flask at −78 °C for 0.5 h and then at 25 °C for 1 h. The resulting solution was next filtered. Pentane (25 mL) was condensed onto the toluene solution, resulting in the formation of yellow powdery product which was then isolated by filtration, washed with a small amount of pentane, and dried under vacuum: yield 75%. Anal. Calcd for $C_{38}H_{32}BF_{15}Zr$: C, 52.12; H, 3.68. Found: C, 52.60; H, 3.39.

$[1,3\text{-}(CMe_3)_2C_5H_3]_2ZrH^+MeB(C_6F_5)_3^-$ (9). $[1,3\text{-}(CMe_3)_2C_5H_3]_2ZrMe_2$ (0.16 g, 0.33 mmol) and $B(C_6F_5)_3$ (0.16 g, 0.31 mmol) were reacted in 15 mL of toluene at room temperature under 1 atm of H_2 for 10 h. Toluene was then removed in vacuo. The resulting solid was washed with a small amount of pentane, collected by filtration, and dried under vacuum: yield 70%. Anal. Calcd for $C_{45}H_{46}BF_{15}Zr$: C, 55.50; H, 4.70. Found: C, 55.75; H, 4.79.

Thermal Stabilities of Complexes 1–4. A C_6D_6 solution of each complex was monitored by ^1H and ^{19}F NMR spectroscopy. Complexes **1–3** showed no noticeable decomposition over several days at room temperature. However, complex **4** underwent clean conversion with a half-life of ca. 10 h at room temperature to $[1,3\text{-}(SiMe_3)_2C_5H_3]_2Zr(Me)(C_6F_5)$ (**10**) and $MeB(C_6F_5)_2$ (**11**), both of which were characterized by multinuclear NMR spectroscopy.

10: NMR (C_6D_6, 20 °C) ^1H δ 6.97 (t, J = 1.8 Hz, 2H), 6.26 (t, J = 2 Hz, 2H), 6.17 (t, J = 2 Hz, 2H), 0.62 (d, $J_{H\text{-}F}$ = 9 Hz, 3H), 0.13 (s, 18H), 0.09 (s, 18H); ^{19}F δ −108.65 (br, 1F, *o*-F), −110.05 (d, J = 31 Hz, 1F, *o*-F), −156.58 (t, J = 19.7 Hz, 1F, *p*-F), −161.77 (br, 1F, m-F), −162.80 (br, 1F, *m*-F).

11: NMR (C_6D_6, 20 °C) ^1H δ 1.32 (br, B-Me); ^{19}F δ −130.00 (d, J = 21.4 Hz, 4F, *o*-F), −146.90 (t, J = 19.9 Hz, 2F, *p*-F), −161.31 (m, 4F, *m*-F).

Additionally, in one of the attempts to grow single crystals of **2** by diffusing pentane into a benzene solution over a course of two weeks, light-yellow, transparent crystals formed. These were found by single crystal diffraction not to be **2** but to be an unusual F-bridged dimeric complex $\{[(1,2\text{-}Me_2C_5H_3)_2ZrCH_3]_2(\mu\text{-}F)\}^+CH_3B(C_6F_5)_3^-$ (**12**) (*vide infra*).

Reaction of $Cp_2Zr(CH_3)CH_2Ph$ with $B(C_6F_5)_3$. The two reagents were reacted in C_6D_6 in an NMR tube at room temperature. ^1H NMR spectroscopy revealed the immediate formation of the cationic complex $Cp_2ZrCH_2Ph^+CH_3B(CF)_3^-$: δ 6.74 (m, *m*-Ph), 6.44 (t, *p*-Ph), 6.20 (d, *o*-Ph), 5.26 (s, Cp), 2.16 (s, CH_2), −1.35 (br, s, CH_3-B).

Reaction of $Cp_2Zr(CH_2Ph)_2$ with $B(C_6F_5)_3$. Reaction of the two reagents at room temperature in C_6D_6 resulted in a red oil. ^1H NMR spectroscopy revealed that it is a mixture of several species, none of which could be clearly identified.

Reaction of $Cp_2Zr(CH_3)Cl$ with $B(C_6F_5)_3$. The reaction of these two reagents at room temperature in C_6D_6 resulted in only a mixture of unidentified species as shown by ^1H NMR spectroscopy.

Reaction of Zirconocene Dialkyls with $B(C_6H_5)_3$. 1. Cp_2ZrMe_2 was mixed with 1 equiv of $B(C_6H_5)_3$ in C_6D_6 at room temperature. The ^1H NMR spectrum of this solution revealed only a mixture of several zirconium-containing species. None of them could be identified as a simple cationic complex analogous to **1**.

2. A similar procedure was carried out with Cp'_2ZrMe_2 and $B(C_6H_5)_3$. After 4 h at room temperature, only starting materials were observed in the ^1H NMR spectrum.

^{13}C Scrambling between 3 and $Cp'_2Zr(^{13}CH_3)_2$. A mixture of $Cp'_2ZrCH_3^+CH_3B(C_6F_5)_3^-$ (**3**) (98.7% ^{12}C at Zr-CH_3) was stirred together with $Cp'_2Zr(CH_3)_2$ (99% ^{13}C at Zr-CH_3) in toluene-d_8. After 4 h at room temperature, ^1H NMR spectroscopy revealed that the ^{13}C labels were evenly distributed among Zr^+-CH_3, B^--CH_3, and $Zr(CH_3)_2$ groups.

Polymerization/Oligomerization of [3-^{13}C] Propylene by Complex 8. A small amount (2–3 mg) of **8** was dissolved in toluene-d_8 in a J-Young NMR tube. The tube was then filled with 1 atm of [3-^{13}C] propylene. Upon vigorous shaking, the polymerization reaction was complete within a few minutes at room temperature. The products were characterized by ^1H and ^{13}C NMR spectroscopy.

Ethylene Polymerization Experiments. Ethylene polymerizations were carried out in a 250-mL flamed, round bottom flask using procedures described previously.[14]

Propylene Polymerization Experiments. Propylene polymerizations were carried out using a quartz Worden vessel and the following procedure. The reaction vessel (a 26 × 2 cm quartz tube, flamed under high vacuum) equipped with a magnetic stirring bar was charged with a small amount of catalyst in the glovebox. The vessel was closed, removed from the glovebox, and attached to the high vacuum line. A measured amount of solvent and propylene was condensed in at −78 °C under vacuum. The reaction mixture was then warmed to, and maintained at, the appropriate reaction temperature. After a measured reaction time, the reaction was quenched by adding a small amount of methanol. The resulting oily liquid polypropylene was washed with methanol and water and then dried under vacuum at 80–100 °C for 10 h. The products are viscous, colorless oils and were analyzed by GPC as well as by ^1H and ^{13}C NMR spectroscopy.

Dimerization of Propylene by Complex 9. 1. In a J-Young NMR tube, a small amount of **9** was dissolved in toluene-d_8. The NMR tube was then filled with 1 atm of propylene. After several hours at 0 °C, ^1H NMR revealed that 2-methyl-1-pentene and 2-methyl-2-pentene (relative ratio of 3 to 2) were the only two products formed. The identity of these two compounds were confirmed by comparing their ^1H NMR data with those of authentic samples.

2. Complex **9** (18.5 mg, 0.020 mmol) was dissolved in 20 mL of toluene in a 50-mL flask. The solution was stirred at 0 °C under 1 atm of propylene for 90 min. The reaction was quenched by adding a small amount of water. The combined yield of 2-methyl-1-pentene and 2-methyl-2-pentene was 1.1 g (estimated by weighing the reaction mixture

Table 1. Summary of Crystal Structure Data for Complexes 2, 3, 4, 6, 8, and 12[a]

complex	2	3	4	6	8	12
formula	$ZrBC_{34}H_{24}F_{15}$	$ZrBC_{40}H_{36}F_{15}$	$ZrBC_{49}H_{53}F_{15}Si_4$	$ZrBC_{59}H_{60}F_{15}$	$ZrBC_{38}H_{32}F_{15}$	$Zr_2BC_{49}H_{45}F_{16}$
crystal system	monoclinic	monoclinic	triclinic	monoclinic	triclinic	triclinic
space group	$P2_1/n$	$P2_1$	$P\bar{1}$	$P2_1/n$	$P\bar{1}$	P_1
a, Å	12.261(2)	9.405(1)	11.639(4)	12.610(5)	11.899(4)	12.308(1)
b, Å	20.010(6)	19.336(3)	12.877(4)	20.995(4)	12.643(4)	13.898(3)
c, Å	13.053(5)	10.382(1)	19.224(4)	21.389(5)	13.681(4)	15.182(2)
α (deg)			77.89(2)		84.47(2)	101.63(1)
β, (deg)	90.80(2)	96.54(1)	74.33(2)	106.13(3)	76.12(3)	90.42(1)
γ (deg)			77.04(3)		65.34(3)	115.22(1)
V, Å^3	3202	1875.7(7)	2669(3)	5440(5)	1816(2)	2288.4(6)
Z	4	2	2	4	2	3
d(calc), g/cm^3	1.700	1.600	1.420	1.404	1.7601	1.641
crystal size, mm	0.2 × 0.3 × 0.6	0.26 × 0.35 × 0.41	0.31 × 0.28 × 0.060	0.3 × 0.2 × 0.2	0.2 × 0.38 × 0.56	0.2 × 0.3 × 0.4
color, habit	yellow, transparent	yellow, transparent	yellow, platy	yellow, equidimensional	yellow, platy	light yellow, prismatic
μ, cm^{-1}	4.46	3.88	3.72	2.84	3.99	5.45
scan type	ω-θ	ω-θ	ω-θ	ω-θ	ω-θ	ω-θ
transmission factors range	0.934–0.862(numerical)	0.91–0.82(numerical)	0.90–0.98	0.90–0.95	0.86–0.93	0.905–0.684
2θ range, (°)	2.0–45 (+h,+k,±l)	2.0–51.9 (±h,–k,+l)	2.0–48.0	2.0–48.0	2.0–48.9	2.0–46 (±h,+k,±1)
intensities (unique, R_i)	4635(4166, 0.016)	5466(3805,0.030)	8785(8362, 0.041)	9235(8795, 0.068)	6330(6025, 0.023)	6795(6359, 0.022)
intensities > 2.58$\sigma(I)$	3261					
> 3$\sigma(I)$		3167	5518	4109	5136	5109
no. of params	539	514	612	617	493	620
R	0.027	0.039	0.043	0.066	0.060	0.031
R_w	0.029	0.046	0.049	0.069	0.082	0.040
max density in ΔF map, e$^-$/Å^3	0.28	0.57	0.74	1.23	1.28	0.40

[a] Diffractometer: Enraf-Nonius, CAD4; temperature for data collection, –120 °C; radiation, graphite monochromator; Mo Kα; λ = 0.71069.

and measuring the molar fraction of these two olefins relative to toluene by ^{1}H NMR).

X-ray Crystallographic Studies of Complexes 2, 3, 4, 6, 8, and 12. Suitable crystals for diffraction studies were grown by slow diffusion of pentane into a saturated benzene solution of each complex at room temperature (complexes **2**, **3**, and **12**), or by slow cooling of a toluene solution of the complex (complexes **4**, **6**, and **8**), and were mounted on a thin glass fiber after being protected with a layer of Paratone oil (Exxon, degassed at 110 °C for 10 h under high vacuum). Data were collected on an Enraf-Nonius CAD4 diffractometer at –120 °C. Final cell dimensions were obtained by a least-squares fit to the automatically centered settings for 25 reflections. Three reference reflections monitored during data collection for each crystal showed no significant variations. Intensity data were all corrected for absorption, anomalous dispersion, and Lorentz and polarization effects. The space group choice for each complex was unambiguously determined. Crystallographic data are summarized in Table 1.

The structures of complexes **2** and **12** were solved by direct methods (SHELXS-86).[27a,b] In **2**, the correct zirconium atom position was deduced from the electron density map. Subsequent least-squares difference Fourier calculations (SHELX-76) revealed atomic positions for the remaining atoms (including all hydrogen atoms). In the final cycle of least-squares, the non-hydrogen atoms were refined with anisotropic thermal coefficients, while the hydrogen atoms were refined with common isotropic thermal parameters. Successful convergence was indicated by the maximum shift/error for the final cycle. A final analysis of variance between observed and calculated structure factors showed no apparent systematic errors. In **12**, the zirconium atom position was deduced from an electron density map. The rest of the nonhydrogen atoms were found subsequently using least-squares difference Fourier calculations and were refined with isotropic thermal coefficients. The hydrogen atoms were refined as idealized positions. The structure of **3** was solved by a combination of Patterson and direct methods.[27d,e] The non-hydrogen atoms were refined anisotropically.

The structure of **4** was solved by direct methods.[27c,e] The disordered carbon atoms of a lattice toluene molecule were refined with isotropic thermal coefficients and converged with site occupancy of 0.52 for the "B"s, and the remaining non-hydrogen atoms were refined anisotropically. Hydrogen atoms were included in fixed positions. The structure of **6** was solved by a Patterson map.[27d,e] Toluene atoms C81–C83 were found from the difference map and were not refined. The methyl groups of the two toluene molecules found on the inversion center were not located in the final difference map. The remaining non-hydrogen solvent atoms and the hydrogen atoms on C22 and C27 were refined isotropically (H22a-b and C27a-c having group isotropic thermal parameters). The remaining non-hydrogen atoms were refined anisotropically. The remaining hydrogen atoms were fixed in "idealized" positions. The highest peaks left in the final difference map were in the vicinity of the toluene molecule C81–C83. The structure of **8** was solved by a combination of the Patterson method and direct methods.[27d,e] The non-hydrogen atoms were refined anisotropically except for the disordered Cp ring carbon atoms which were refined isotropically.

All calculations were performed using the TEXSAN crystallographic software package of Molecular Structure Corporation.

Results and Discussion

I. Cationic Zirconocene Alkyl and Hydride Complexes. Synthesis and Spectroscopy. The reaction of tris(pentafluorophenyl)borane with a variety of zirconocene dimethyl complexes proceeds rapidly and quantitatively (by NMR) at room temperature in noncoordinating solvents to yield, after recrystallization, methyltriarylborate complexes (eq 2). Reaction with excess of $B(C_6F_5)_3$ does not effect the removal of the second methyl group, even after extended periods of reaction.

$$L_2Zr(CH_3)_2 + B(C_6F_5)_3 \xrightarrow{\text{benzene or pentane}} \underset{\textbf{1-4}}{L_2ZrCH_3^+CH_3B(C_6F_5)_3^-} \quad (2)$$

1. L = η^5-C_5H_5 (Cp)
2. L = η^5-1,2-$Me_2C_5H_3$ (Cp")
3. L = η^5-C_5Me_5 (Cp')
4. L = η^5-1,3-$(SiMe_3)_2C_5H_3$ (TMS_2Cp)

Interestingly, when $[1,3\text{-}^t\mathrm{Bu}_2\mathrm{C}_5\mathrm{H}_3]_2\mathrm{ZrMe}_2$ is exposed to $B(C_6F_5)_3$, the expected simple cationic methyl complex $[1,3\text{-}^t\mathrm{Bu}_2\mathrm{C}_5\mathrm{H}_3]_2\mathrm{ZrMe}^+\mathrm{MeB}(\mathrm{C}_6\mathrm{F}_5)_3^-$ (**5**) is not obtained. Instead, the ring-metalated, metallacyclic complex **6**, which apparently results from an intramolecular C–H activation reaction of **5**, was isolated in quantitative yield (by NMR) (eq 3). The formation of **6** is rapid (eq 3 is complete in less than 1 h at room temperature).

(27) (a) Sheldrich, G. M. SHELXS-86 in *Crystallographic Computing*; Sheldrich, G. M., Kruger, C., Goddard, R. Eds.; Oxford University Press: 1985, pp 175–189. (b) Sheldrich, G. M. *SHELX-76, A Program for Crystal Structure Determination*; University Chemical Laborotory, Cambridge, England, 1976. (c) Gilmore, C. J. MITHRIL—an integrated direct methods computer program In *Journal of Applied Crystallography:* University of Glasgow: Scotland, 1984; 17, pp 42–46. (d) Calbrese, J. C. PHASE—Patterson Heavy Atom Solution Extractor. University of Wisconsin-Madison, Ph.D. Thesis, 1972. (e) Beurskens, P. T. DIRDIF: Direct Methods for Difference Structures—an automatic procedure for phase extension and refinement of difference structure factors. Technical Report 1984/1 Crystallography Laboratory, Toernooiveld, 6525 Ed Nijmegan, Netherlands.

Table 2. ^{1}H NMR Data (C_6D_6, 20 °C)

compound	assignment	δ, ppm	coupling, Hz
$Cp_2ZrCH_3^+CH_3B(C_6F_5)_3^-$	C_5H_5	5.37 (s)	
(1)	$ZrCH_3$	0.26 (s)	
	BCH_3	0.10 (br, s)	
$Cp''_2ZrCH_3^+CH_3B(C_6F_5)_3^-$	$C_5H_3Me_2$	5.49 (t, 2H)	$^3J_{HH}$ = 2.8
(2)	$C_5H_3Me_2$	5.23 (t, 2H)	$^3J_{HH}$ = 3.2
	$C_5H_3Me_2$	4.78 (t, 2H)	$^3J_{HH}$ = 2.8
	$C_5H_3Me_2$	1.51 (s, 6H)	
	$C_5H_3Me_2$	1.20 (s, 6H)	
	$ZrCH_3$	0.08 (s)	
	BC_3	0.02 (br, s)	
$Cp'_2ZrCH_3^+CH_3B(C_6F_5)_3^-$	C_5Me_5	1.37 (s)	
(3)	$ZrCH_3$	0.29 (s)	
	BCH_3	−0.30 (br, s)	
$[1,3\text{-}TMS_2C_5H_3]_2ZrCH_3^+CH_3B(C_6F_5)_3^-$ (4)	$C_5H_3(SiMe_3)_2$	6.91 (s, 2H)	
	$C_5H_3(SiMe_3)_2$	6.27 (s, br, 2H)	
	$C_5H_3(SiMe_3)_2$	5.90 (s, br, 2H)	
	$ZrCH_3$	0.72 (s)	
	BCH_3	0.39 (s, br)	
	$C_5H_3(SiMe_3)_2$	−0.001 (s, 36H)	
$(1,3\text{-}^tBu_2C_5H_3)(^tBuC_5H_3CMe_2\overline{CH_2})Zr^+MeB(C_6F_5)_3^-$ (6)	$(CMe_3)_2C_5H_3$	6.71 (t, 1H)	$^3J_{HH}$ = 2.4
	$(CMe_3)_2C_5H_3$	6.38 (s, br, 1H)	
	$(CMe_3)_2C_5H_3$	5.52 (t, 1H)	$^3J_{HH}$ = 2.4
	$(CMe_3C_5H_3C(Me_2)CH_2$	4.86 (m, 1H)	
	$(CMe_3C_5H_3C(Me_2)CH_2$	4.78 (m, 1H)	
	$(CMe_3C_5H_3C(Me_2)CH_2$	4.33 (s, br, 1H)	
	$(CMe_3C_5H_3C(Me_2)CH_2$	1.41 (s, 3H)	
	CMe_3	1.02 (s, 9H)	
	CMe_3	0.96 (s, 9H)	
	CMe_3	0.81 (s, 9H)	
	BCH_3	0.53 (s, br)	
	$(CMe_3C_5H_3C(Me_2)CH_2$	0.52 (s, 3H)	
	$(CMe_3C_5H_3C(Me_2)CH_2)$	−2.61 (d, 1H)	$^3J_{HH}$ = 10
$Cp'_2ZrH^+MeB(C_6F_5)_3^-$ (7)	ZrH	7.70 (s	
	C_5Me_5	1.48 (s)	
	BCH_3	0.10 (s, br)	
$Cp'_2ZrH^+HB(C_6F_5)_3^-$ (8)[a]	ZrH	8.18 (s)	
	BH	3.98 (d, br)	
	C_5Me_5	1.50 (s)	
$[1,3\text{-}^tBu_2C_5H_3]_2ZrH^+MeB(C_6F_5)_3^-$ (9)	$(CMe_3)_2C_5H_3$	6.14 (d, 2H)	$^3J_{HH}$ = 2.0
	$(CMe_3)_2C_5H_3$	5.72 (s, 2H)	
	$(CMe_3)_2C_5H_3$	5.23 (s, 2H)	
	ZrH	4.18 (s)	
	$(CMe_3)_2C_5H_3$	1.03 (s, 18H)	
	$(CMe_3)_2C_5H_3$	0.89 (s, 18H)	
	BCH_3	0.39 (s, br)	

[a] In toluene-d_8, 0 °C.

The generation of 1 equiv of CH_4 has been confirmed by ^{1}H NMR spectroscopy.

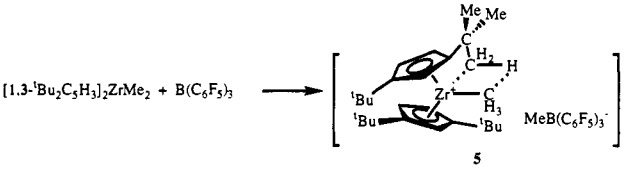

(3)

Cationic methyl complex **3** also undergoes rapid, stepwise hydrogenolysis to yield mono- and dihydrido complexes **7** and **8**, respectively (eq 4).[28] The use of pentane as the solvent is essential for the isolation of the sparingly soluble monohydrido species **7** (which precipates from the reaction medium immediately upon formation). Alternatively, **8** can be prepared by $B(C_6F_5)_3$ hydride abstraction from Cp'_2ZrH_2. Such hydrido species are doubtless key intermediates in polymerization chain-transfer processes such as β-H elimination and molecular weight control by H_2, and previously have been isolable only as Lewis base adducts.[29] The

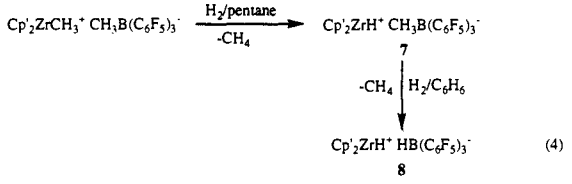

(4)

transformation of **7** to **8** most likely proceeds through an initial Zr–H/B–CH_3 exchange process, followed by the hydrogenolysis of the Zr–CH_3 bond (eq 5). Similarly, complex **6** undergoes

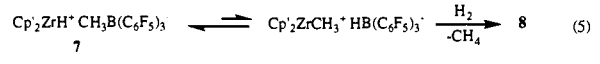

(5)

rapid hydrogenolysis to afford monohydrido complex **9**. However, unlike **7**, complex **9** does not undergo further reaction with H_2, even after extended periods of exposure (eq 6). It is reasonable that the bulky ancillary ligands of **9** impede Zr–H/B–CH_3 exchange.

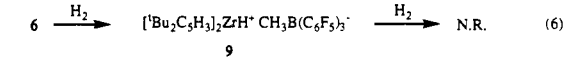

(6)

(28) Yang, X.; Stern, C. L.; Marks, T. J. *Angew. Chem., Int. Ed. Engl.* **1992**, *31*, 1375–1377.

Table 3. ^{13}C NMR Data (C_6D_6, 20 °C)

compound	assignment	δ, ppm	coupling, Hz
$Cp_2ZrCH_3^+CH_3B(C_6F_5)_3^-$	C_6F_5	148.63 (d, 6C)	$^1J_{CF}$ = 241.1
(1)	C_6F_5	139.62 (d, 3C)	$^1J_{CF}$ = 247.9
	C_6F_5	137.57 (d, 6C)	$^1J_{CF}$ = 245.2
	C_6F_5	123.16 (br, s, 3C)	
	C_5H_5	114.01 (d)	$^1J_{CH}$ = 176.5
	$ZrCH_3$	40.93 (q)	$^1J_{CH}$ = 122.6
	BCH_3	26.10 (br, s)	
$Cp''_2ZrCH_3^+CH_3B(C_6F_5)_3^-$	$C_5H_3Me_2$	115.77	
(2)[a]	$C_5H_3Me_2$	112.08	
	$C_5H_3Me_2$	106.77	
	$ZrCH_3$	44.60 (s)	
	BCH_3	22.80 (s, br)	
	$C_5H_3\mathit{Me}_2$	12.48 (s)	
$Cp'_2ZrCH_3^+CH_3B(C_6F_5)_3^-$	C_5Me_5	124.01 (s)	
(3)	$ZrCH_3$	50.36 (q)	$^1J_{CH}$ = 121.5
	BCH_3	14.34 (br, s)	$^1J_{CH}$ = 118
	$C_5\mathit{Me}_5$	11.02 (q)	$^1J_{CH}$ = 127.4

[a] $^{13}C\{^1H\}$.

Complexes **1–4** and **6–9** have been characterized by standard spectroscopic/analytical techniques (Tables 2–4). Some were also characterized crystallographically (*vide infra*). There are several interesting spectroscopic features of these cationic zirconium complexes. In the ^{13}C NMR spectra, the cationic methyl complexes exhibit a marked downfield shift of the Zr–$^{13}CH_3$ signal from the corresponding neutral zirconocene dimethyl precursors. A similar trend has also been observed in a series of closely related cationic thorium complexes.[30] This feature doubtless originates from the electron-deficient character of such cationic species. It may thus be used as a key diagnostic tool in probing the formation of similar cationic active species in more complicated catalytic systems involving zirconocene and Lewis acidic cocatalysts such as methylalumoxane or dehydroxylated alumina (DA) (see more details in the Discussion section). It can also be seen in Table 3 that one-bond $J_{^{13}C-^1H}$ values for the Zr–CH_3 groups of the present zirconocene cations are unexceptional for early transition metal methyl complexes. Hence, there is no evidence for hybridization changes that might be associated with an α-"agostic" C–H interaction. Several of the solid cationic complexes were also investigated by ^{13}C CPMAS NMR spectroscopy. In all cases, solution phase and solid state Zr–CH_3 chemical shifts are identical within experimental error. This gives assurance that diffraction-derived solid state and solution phase structures are quite similar.

Related to the cationic zirconocene electron deficiency, complexes **7** and **8** both exhibit a downfield shift in the ^1H NMR of the Zr–H signal versus the neutral dihydride precursor (δ = 7.70 (**7**) and 8.18 (**8**) vs δ = 7.46 for Cp'_2ZrH_2 in C_6D_6).[24] In the IR spectra (Nujol mulls), the ν_{Zr-H} modes of the cationic hydrides are shifted to higher frequencies: **7**, ν_{Zr-H} = 1642 (ν_{Zr-D} = 1174) cm^{-1} and **8**, ν_{Zr-H} = 1663, 1604 cm^{-1}. The analogous values for Cp'_2ZrH_2[24] and $Cp'_2Zr(H)O^tBu$[24] are 1555 and 1582 cm^{-1}, respectively. In addition, the $^1H/^{13}C$ NMR signals of the $CH_3BR_3^-$ and HBR_3^- groups reveal the expected $^{10}B/^{11}B$ quadrupolar-broadening.[31] The $^{13}C-^1H$ coupling constant of the $^{13}CH_3BR_3^-$ group in **3** (118 Hz) argues for unexceptional sp^3 hybridization at the methyl carbon atom, and this has been confirmed crystallographically (*vide infra*).

The reaction of $B(C_6F_5)_3$ with $Cp_2Zr(CH_3)CH_2Ph$ in C_6D_6 also results in the formation of the cationic complex $Cp_2Zr-CH_2Ph^+CH_3B(C_6F_5)_3^-$ (eq 7). The cation ^1H NMR spectroscopic features are similar to the zirconium benzyl complex reported by Jordan et al. using BPh_4^- as the counterion, with a high-field shift of the ortho hydrogen atoms (see Experimental Section) of the benzyl group, suggesting η^3-coordination of benzyl group to Zr.[32]

$$Cp_2Zr(CH_3)CH_2Ph + B(C_6F_5)_3 \rightarrow Cp_2Zr(\eta^n\text{-}CH_2Ph)^+\ CH_3B(C_6F_5)_3^- \quad (7)$$

In contrast, the reactions of $Cp_2Zr(CH_2Ph)_2$ or $Cp_2Zr(CH_3)Cl$ with $B(C_6F_5)_3$ at room temperature are complex and do not give products which can be identified as zirconocene cations by ^1H NMR. The different behavior of $Cp_2Zr(CH_3)CH_2Ph$ and $Cp_2Zr(CH_2Ph)_2$ suggests that a benzyl group is less effective than a methyl or a hydride group in forming a stable borate anion. Interestingly, Pellechia et al. have recently shown that $PhCH_2B(C_6F_5)_3^-$ can serve as an η^6-ligand in cationic zirconium complexes with a more open coordination environments.[33]

In contrast to $B(C_6F_5)_3$, BPh_3 does not abstract a methyl group from Cp'_2ZrMe_2 to form an identifiable cation. The reaction with Cp_2ZrMe_2 only results in the formation of several unidentified, noncationic species.

II. Zirconocene Cations. Reaction Chemistry and Thermal Stability. Compared to the neutral dimethyl or dihydrido precursors, the cationic zirconocene complexes have a much more open coordination environment and potentially greater electrophilicity. This is expected to render them chemically far more reactive and is doubtless the origin of their high catalytic activities (*vide infra*). However, to be used as catalysts such complexes should also be sufficiently thermally stable to avoid self-destruction during polymerization processes at high temperatures. We have studied the thermal stability of these cationic complexes and have discovered several interesting reaction pathways.

It is found that the thermal stability of $L_2ZrMe^+MeB(C_6F_5)_3^-$ complexes is extremely sensitive to the type of ancillary ligands surrounding the metal center. Thus, complexes **1–3** are stable for days at room temperature under an inert atmosphere as toluene or benzene solutions without noticeable decomposition. However, **4** has a half-life of only ~10 h at room temperature, while complex **5** could not even be isolated under such conditions (NMR monitoring of the reaction reveals that **5** has a half-life of ca. ~5 min at room temperature). Three different reaction pathways have been identified.

A. Ligand Redistribution. The moderately stable complex **4** slowly undergoes decomposition to $[1,3\text{-}TMS_2C_5H_3]_2Zr(Me)(C_6F_5)$ (**10**) and $MeB(C_6F_5)_2$ (**11**) over a course of 1 day at room temperature in C_6D_6 (eq 8). Both of the products were characterized by *in situ* ^1H and ^{19}F NMR spectroscopy (see Experimental Section for details). This is a very interesting result,

$$\underset{\mathbf{4}}{(TMS_2Cp)_2ZrMe^+MeB(C_6F_5)_3^-} \rightarrow \underset{\mathbf{10}}{(TMS_2Cp)_2Zr(Me)C_6F_5} + \underset{\mathbf{11}}{MeB(C_6F_5)_2} \quad (8)$$

because it reveals that **4** is probably formed as the *kinetic* product rather than the *thermodynamic* one in eq 2. A similar decomposition pattern has also been observed in the related cationic actinide complex $Cp'_2ThMe^+BPh_4^-$ [35] and in the in situ-generated, base-coordinated complexes $[L_2ZrMe(NMe_2Ph)_n]^+B(4\text{-}C_6H_4F)_4^-$ (L = Cp, TMSCp, MeCp, Cp').[12f]

B. Intramolecular C–H Activation. This reaction pathway is shown in eq 3. The facility of this process is remarkable because although the M–CH_3 (M = Zr, Th) bond in a cationic metallocene complex readily undergoes reaction with an aryl C–H bond of

(29) Jordan, R. F.; Bajgur, C. S.; Dasher, W. E.; Rheingold, A. L. *Organometallics* **1987**, *6*, 1041–1051.

(30) (a) Yang, X.; Stern, C. L.; Marks, T. J. *Organometallics* **1991**, *10*, 840–842. (b) Lin, Z.; Le Marechal, J.-F.; Sabat, M.; Marks, T. J. *J. Am. Chem. Soc.* **1987**, *109*, 4127–4129.

(31) (a) Nöth, H.; Wrackmeyer, B. *Nuclear Magnetic Resonance Spectroscopy of Boron Compounds*; Springer Verlage: Berlin, 1978; Chapters 4 and 7. (b) Onak, T. *Organoborane Chemistry*; Academic Press: New York, 1975; Chapter 2.

(32) Jordan, R. F.; LaPoint, R. E.; Bajgur, C. S.; Echols, S. F.; Willett, R. *J. Am. Chem. Soc.* **1987**, *109*, 4111–4113.

(33) Pellechia, C.; Grassi, A.; Immirzi, A. *J. Am. Chem. Soc.* **1993**, *115*, 1160–1162.

Table 4. ^{19}F NMR Data (C_6D_6, 20 °C)

compound	assignment	δ, ppm	coupling, Hz
$Cp_2ZrCH_3^+CH_3B(C_6F_5)_3^-$	*o*-F	−133.73 (d)	$^3J_{FF}$ = 21.7
(**1**)	*p*-F	−158.57 (t)	$^3J_{FF}$ = 21.0
	m-F	−164.06 (t)	$^3J_{FF}$ = 18.3
$Cp''_2ZrCH_3^+CH_3B(C_6F_5)_3^-$	*o*-F	−133.50 (d)	$^3J_{FF}$ = 23.2
(**2**)	*p*-F	−158.90 (t)	$^3J_{FF}$ = 20.7
	m-F	−164.19 (t)	$^3J_{FF}$ = 18.7
$Cp'_2ZrCH_3^+CH_3B(C_6F_5)_3^-$	*o*-F	−130.70 (d)	$^3J_{FF}$ = 21.2
(**3**)	*p*-F	−158.20 (t)	$^3J_{FF}$ = 19.7
	m-F	−163.09 (br)	
$[1,3\text{-}TMS_2C_5H_3]_2ZrCH_3^+CH_3B(C_5F_5)_3^-$ (**4**)	*o*-F	−131.83 (d)	$^3J_{FF}$ = 19.7
	p-F	−159.31 (t)	$^3J_{FF}$ = 20.3
	m-F	−164.60 (br)	
$[1,3\text{-}^tBu_2C_5H_3][CMe_3C_5H_3C(Me_2)CH_2]Zr^+MeB(C_6F_5)_3^-$ (**6**)	*o*-F	−132.59 (d)	$^3J_{FF}$ = 21.1
	p-F	−159.58 (t)	$^3J_{FF}$ = 20.0
	m-F	−164.24 (b)	
$Cp'_2ZrH^+MeB(C_6F_5)^-$ (**7**)	*o*-F	−132.94 (d)	$^3J_{FF}$ = 22.6
	p-F	−159.80 (t)	$^3J_{FF}$ = 20.6
	m-F	−176.02 (m)	
$Cp'_2ZrH^+HB(C_6F_5)_3^-$ (**8**)	*o*-F	−137.08 (br, s)	
	p-F	−160.75 (t)	$^3J_{FF}$ = 20.6
	m-F	−168.36 (br, s)	
$[1,3\text{-}^tBu_2C_5H_3]_2ZrH^+MeB(C_6F_5)_3^-$ (**9**)	*o*-F	−132.29 (d)	$^3J_{FF}$ = 21.4
	p-F	−159.82 (t)	$^3J_{FF}$ = 20.6
	m-F	−164.45 (t)	$^3J_{FF}$ = 18.3

Scheme 1. Possible Mechanisms for the Formation of Complex **12**

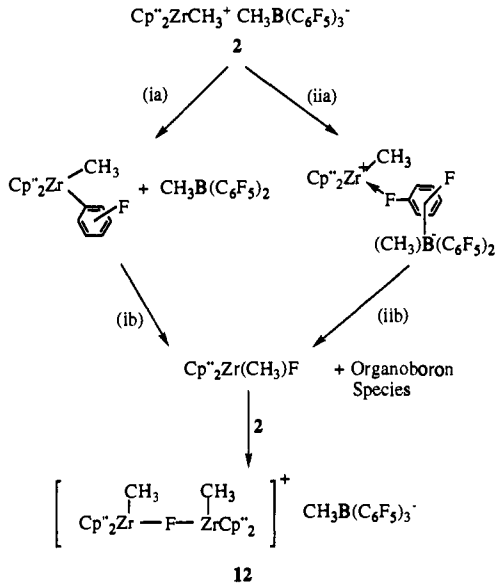

12

BPh_4^- [12j] or with the methyl protons of toluene solvent,[34] this is the first example where such a metal center has been shown to react with an *unactivated* CH_3 group. The open Zr(IV) coordination environment, the high Lewis acidity at the metal center, and the intramolecular accessibility of the unactivated methyl group are doubtless important factors which promote this reaction under such mild conditions. As a matter of fact, this behavior closely resembles that of neutral Cp'_2LuCH_3, which effects reversible C–H activation of the CH_4 molecule.[13]

C. Fluoride Abstraction. Prolonged standing of a solution of **2** in benzene at 25 °C over several weeks results in the formation of the fluoride-bridged complex $[Cp''_2(CH_3)Zr(\mu\text{-}F)Zr(CH_3)Cp''_2]^+CH_3B(C_6F_5)_3^-$ (**12**), as shown by an X-ray crystallographic study (*vide infra*). Complex **12** can be viewed as an adduct between **2** and $Cp''_2Zr(CH_3)F$. The latter is apparently a thermolysis product of **2**. There are two reasonable mechanisms for the formation of $Cp''_2Zr(CH_3)F$ (Scheme 1). In mechanism (i), the first step involves the transfer of an aryl ring to the zirconium metal center to form $Cp'_2Zr(CH_3)C_6F_5$ and $CH_3B(C_6F_5)_2$. Analogous reactions have been observed in several complexes, including the decomposition of **4** (*vide supra*).[12f,35] The subsequent fluoride transfer may involve intramolecular *o*-fluoride elimination from $Cp'_2Zr(CH_3)(C_6F_5)$. Reactions analogous to this have been observed in the thermolyses of $Li(C_6F_5)$, $Al(C_6F_5)_3{\cdot}OEt_2$,[36] and $Cp_2Ti(C_6F_5)_2$.[37] This process may also be accelerated by the presence of $MeB(C_6F_5)_2$ which could promote the formation of the reasonably more reactive cationic complex $Cp''_2Zr(C_6F_5)^+Me_2B(C_6F_5)_2^-$.

A second conceivable mechanism (mechanism (**ii**)) could involve a direct abstraction of a fluoride from the $CH_3B(C_6F_5)_3^-$ anion by the zirconium cation. There is, to our knowledge, no precedent in the literature for such a reaction pathway. However, it is not unreasonable considering the high electronic and coordinative unsaturation of the hard zirconium cation and therefore cannot be ruled out. Not surprisingly, heating dramatically increases the thermolysis rate. Thus, complex **2** decomposes into several unidentified products over a course of ~1 h at 80 °C in toluene-d_8 solution.

D. Intermolecular C–H Activation. In addition to the above reaction pathways, the hydrido complexes **7** and **8** undergo rapid H/D exchange with the deuterated aromatic solvents (eq 9) ($t_{1/2}$ for the disappearance of the Zr–H signal is ~12 h and ~6 min for **7** and **8**, respectively in C_6D_6), typical behavior for highly coordinatively unsaturated and electron-deficient f-element hydride complexes.[13,14,34] In contrast, the Lewis base-coordinated complexes $Cp_2ZrH(L)_2^+BPh_4^-$ (L = THF, PMe_3) do not undergo such rapid exchange.[29] The rapid incorporation of deuterium into

$$Cp'_2ZrH^+\,HB(C_6F_5)_3^- \underset{}{\overset{C_6D_6}{\rightleftharpoons}} Cp'_2ZrD^+\,HB(C_6F_5)_3^- \quad (9)$$
$$\Big\Vert\, C_6D_6$$
$$Cp'_2ZrD^+\,DB(C_6F_5)_3^-$$

the $H\text{-}B(C_6F_5)_3^-$ anion also indicates rapid exchange of the Zr–H/B–H funtionalities (direct B–H/C_6D_6 exchange is not expected).

III. Crystal Structures of the Cationic Zirconium Complexes 2, 3, 4, 6, 8, and 12. A. Structures of Complexes 2, 3, and 4. The structures of **2, 3,** and **4** are closely related and will be discussed together.

(34) Yang, X. Ph.D. Dissertation, Northwestern University; 1991.

(35) Lin, Z. Ph.D. Dissertation, Northwestern University, 1988.

(36) Cohen, S. E.; Massey, A. G. *Adv. Fluorine Chem.* **1970**, *6*, 149–162.

(37) Treichel, P. M.; Stone, F. G. A. *Adv. Organomet. Chem.* **1964**, *1*, 143–216.

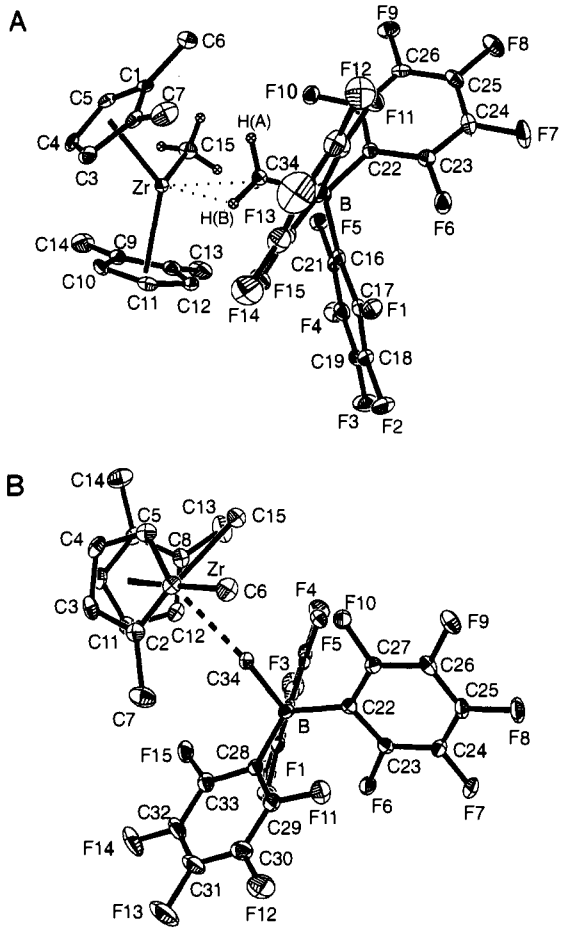

Figure 1. Perspective ORTEP drawings of the molecular structure of complex **2**. Thermal ellipsoids are drawn at the 35% probability level. (A) Viewed nearly perpendicular to the ring Cg-Zr-ring Cg plane. (B) Viewed approximately along the ring Cg–ring Cg vector. Protons on the Cp rings and Cp-Me groups are omitted for clarity. The dotted lines are drawn as a guide to the eye.

Table 5. Selected Bond Distances (Å) and Angles (deg) for $(1,2\text{-}Me_2C_5H_3)_2ZrCH_3{}^+CH_3B(C_6F_5)_3{}^-$ (**2**)

	Bond Distances		
Zr–C1	2.543(3)	Zr–C2	2.550(3)
Zr–C3	2.469(3)	Zr–C4	2.483(3)
Zr–C5	2.487(3)	Zr–C8	2.563(3)
Zr–C9	2.524(3)	Zr–C10	2.475(3)
Zr–C11	2.455(3)	Zr–C12	2.498(3)
Zr–C15	2.252(4)	C15–H15A	0.98(4)
C15–H15B	0.89(4)	C15–H15C	0.99(4)
C16–B	1.665(5)	C22–B	1.643(5)
C28–B	1.651(5)	C34–B	1.663(5)
Zr–C34	2.549(3)	Zr–H34A	2.71(3)
Zr–H34B	2.25(3)	Zr–H34C	2.30(3)
C34–H34A	1.00(3)	C34–H34B	0.98(3)
C34–H34C	0.97(3)		
	Angles		
Zr–C34–B	161.8(2)	C16–B–C22	106.5(3)
C16–B–C28	114.3(3)	C16–B–C34	108.7(3)
C22–B–C28	112.0(3)	C22–B–C34	112.7(2)
C28–B–C34	102.8(3)	Zr–H34B–C34	96(2)
Zr–C15–H15A	110(2)	Zr–C15–H15B	118(2)
Zr–C15–H15C	116(2)	Zr–C34–H34A	89(2)
Zr–C34–H34B	61(2)	Zr–C34–H34C	64(2)
C15–Zr–C34	92.0(1)	Zr–C34–B	161.8(2)

1. General Description. The solid state structures of **2**, **3**, and **4** as derived from the single crystal X-ray diffraction studies all consist of ion pairs in which the cation is associated with the anion through a highly unsymmetrical $Zr\cdots CH_3$–B bridge (Figures 1–3). Important distances and angles for each complex are

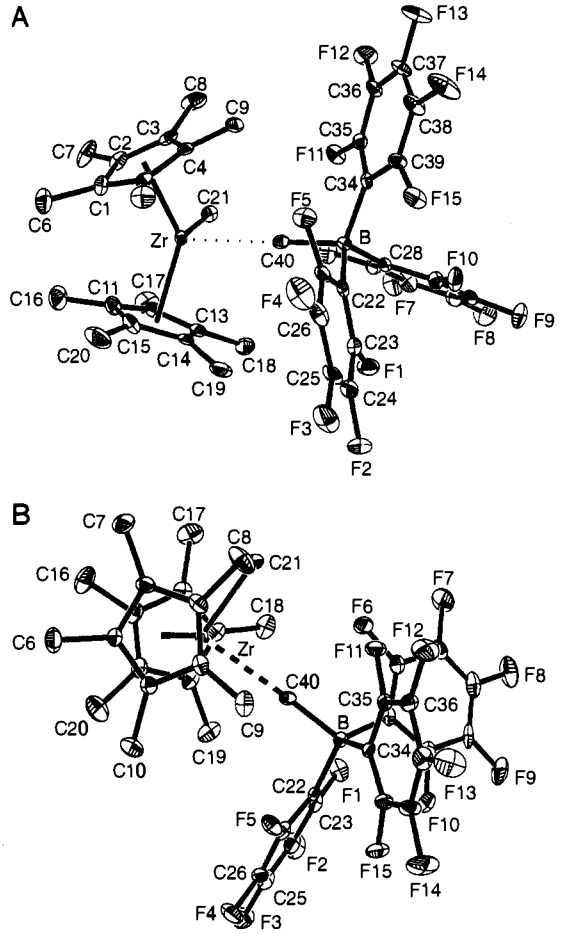

Figure 2. Perspective ORTEP drawings of the molecular structure of complex **3**. Thermal ellipsoids are drawn at the 50% probability level. (A) Viewed nearly perpendicular to the ring Cg-Zr-ring Cg plane. (B) Viewed approximately along the ring Cg–ring Cg vector. The dotted lines are drawn as a guide to the eye.

Table 6. Selected Bond Distances (Å) and Angles (deg) for $(Me_5C_5)_2ZrCH_3{}^+CH_3B(C_6F_5)_3{}^-$ (**3**)

	Bond Distances		
Zr–C1	2.558(7)	Zr–C2	2.540(7)
Zr–C3	2.551(7)	Zr–C4	2.534(6)
Zr–C5	2.509(6)	Zr–C11	2.511(7)
Zr–C12	2.526(7)	Zr–C13	2.557(7)
Zr–C14	2.549(7)	Zr–C15	2.530(7)
Zr–C21	2.223(6)	C22–B	1.666(9)
C23–C24	1.38(1)	C28–B	1.64(1)
C29–C30	1.39(1)	C30–C31	1.36(1)
C34–B	1.655(9)	C40–B	1.66(1)
	Angles		
C22–B–C28	111.5(5)	C22–B–C34	114.6(5)
C22–B–C40	101.7(5)	C28–B–C34	104.2(5)
C28–B–C40	114.3(5)	C34–B–C40	110.9(5)
Zr–C40–B	176.6(4)		

summarized in Tables 5–7, respectively. The formally ionic character of these complexes is unambiguously established by the much longer $Zr\cdots CH_3$(bridging) distance than the $Zr–CH_3$-(terminal) distance in each complex (The differences are 0.297, 0.377, and 0.407 Å, respectively, for complexes **2**, **4**, and **3**) and by the relatively "normal" $B–CH_3$ distances (more details will be discussed in the following sections).

2. Structural Features of the Metallocene Cations. The zirconium cation in each of the three complexes adopts a normal "bent sandwich" configuration. However, the three structures differ from each other as well as from neutral Cp_2ZrMe_2 in several key structural parameters (Table 8). Thus, the Cg–Zr–Cg angles in **2** and **4** (131.1 and 132.1°, respectively) are similar, and are

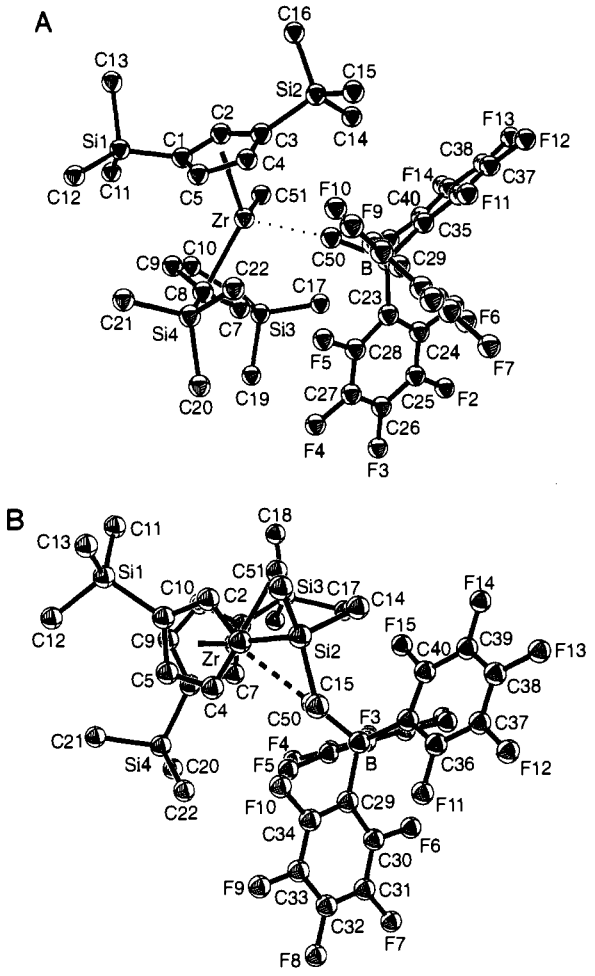

Figure 3. Perspective ORTEP drawings of the molecular structure of complex **4**. Thermal ellipsoids are drawn at the 50% probability level. (A) Viewed nearly perpendicular to the ring Cg-Zr-ring Cg plane. (B) Viewed approximately along the ring Cg–ring Cg vector. The dotted lines are drawn as a guide to the eye.

Table 7. Selected Bond Distances (Å) and Angles (deg) for $(1,3\text{-}TMS_2C_5H_3)_2ZrCH_3{}^+CH_3B(C_6F_5)_3{}^-$ (**4**)

	Bond Distances		
Zr–C1	2.516(5)	Zr–C2	2.520(5)
Zr–C3	2.550(5)	Zr–C4	2.510(5)
Zr–C5	2.4775)	Zr–C6	2.591(5)
Zr–C7	2.537(5)	Zr–C8	2.492(5)
Zr–C9	2.461(5)	Zr–C10	2.504(5)
Zr–C50	2.625(5)	C23–B	1.657(8)
C29–C50–B	1.653(7), 1.699(7)	C35–B	1.645(7)
	Angles		
Si1–C1–C2	124.1(4)	Si1–C1–C5	127.5(4)
C2–C1–C5	105.2(4)	Si2–C3–C2	125.6(4)
Si2–C3–C4	128.1(4)	C2–C3–C4	104.7(4)
Si4–C8–C7	126.4(4)	Si4–C8–C9	127.5(4)
C7–C8–C9	104.4(4)	Si3–C6–C7	126.1(4)
Si3–C6–C10	127.8(4)	C7–C6–C10	104.2(4)
C50–Zr–C51	97.6(2)	Zr–C50–B	171.1(3)
C23–B–C29	105.8(4)	C23–B–C35	113.4(4)
C23–B–C50	106.5(4)	C29–B–C35	111.9(4)
C29–B–C50	112.9(4)	C35–B–C50	106.4(4)

close to that in Cp_2ZrMe_2 (132.5°).[38] On the other hand, the Cg–Zr–Cg angle in **3** is more than 4° larger. This is no doubt a result of the sterically more encumbered Cp′ ligand. The TMS_2-Cp ligands in **4**, although also sterically bulky, can be disposed in such a way as to minimize eclipsing interactions between TMS substituents (Figure 3B). Hence the Cg–Zr–Cg angle is unexceptional. Consistent with these steric arguments, there is also a steady increase in the Zr–C(ring)(av) distance on going from **2** to **4** to **3** (2.500, 2.516, and 2.537 Å, respectively).

Table 8. Comparison of Selected Structural Parameters for the Zirconium Cations **2**, **3**, and **4**[b]

complex	Zr–CH_3 (terminal) (Å)	Zr–CH_3 (bridging) (Å)	Zr–C (ring, av) (Å)	∠Cg–Zr–Cg (deg)
2	2.252(4)	2.549(3)	2.500(2)	131.1(3)
4	2.248(5)	2.625(5)	2.516(3)	132.1
3	2.223(6)	2.640(7)	2.537(3)	136.6
Cp_2ZrMe_2[a]	2.273(5), 2.280(5)		2.525(12)	132.5

[a] From ref 38. [b] Data for Cp_2ZrMe_2 are also included for comparison.

Table 9. Comparison of Selected Structural Parameters for the Anions in **2**, **3**, **4**, and **12**

complex	B–CH_3 (Å)	B–C (aryl, av) (Å)	∠CH_3–Zr–C(aryl,av) (deg)
2	1.663(5)	1.653(3)	108.1
4	1.699(7)	1.652(5)	108.6
3	1.66(1)	1.66(1)	109.0
12	1.638(5)	1.665(3)	108.8

In regard to Zr–CH_3(terminal) distances, there is a steady decrease in bond length on going from **2** to **4** to **3** (2.252(4), 2.248(5), and 2.223(6) Å, respectively). This contraction can be rationalized in terms of complementary electrostatic and coordinative saturation effects. First, it is reasonable that the Zr–CH_3 distance should be affected by the steric bulk of the Cp ligands such that the more encumbered the Cp rings (which exhibit greater average Zr–C(ring) distances) should correlate with shorter Zr–CH_3 distances (stronger Zr–CH_3 bonding in response to weaker Zr–Cp bonding). Secondly, the Zr–CH_3 distance should also be affected by the electronic characteristics of the metal center in such a way that more electron-deficient/coordinatively unsaturated metal centers are accompanied by stronger Zr–CH_3 bonding (shorter Zr–CH_3 distances). The second effect is apparent in a series of metallocene complexes where the Cp ligands are kept constant, while the electronic character of the metal center is modified by change of anion or coordinated Lewis base. Thus, on proceeding from $Cp'_2ZrMe^+MeB(C_6F_5)_3{}^-$ (**3**), to $(Me_4C_5Et)_2ZrMe^+(\eta^1\text{-}H_{12}C_2B_9)^-$,[12j] to $Cp'_2ZrMe(THT)^+BPh_4{}^-$ (THT = tetrahydrothiophene),[12g] the Zr–CH_3 distance appears to increase from 2.223(6) to 2.240(4) to 2.242(8) Å. Both $(C_2B_9H_{12})^-$ and THT should be more electron-donating than $MeB(C_6F_5)_3{}^-$. In addition, the Zr–CH_3 distances in **2**, **3**, and **4** are significantly shorter than those in neutral Cp_2ZrMe_2 (2.273(5), 2.280(5) Å; Table 8) as well as that in $Cp_2ZrMe(THF)^+BPh_4{}^-$ (2.256(10) Å).[39] In fact, the Zr–CH_3 distance in **3** is the shortest among all structurally characterized cationic zirconocene methyl complexes.[11,12]

3. Structural Features of the Anion. Cationic complexes **2**, **3**, and **4** as well as **12** share the common anion $MeB(C_6F_5)_3{}^-$, which has a pseudotetrahedral geometry (**II**). However, unlike **2**, **3**, and **4**, the anion is not closely associated with any particular cation in the solid state structure of **12** (Figure 7, *vide infra*).

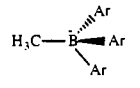

II

Therefore, by comparing the structural parameters of the "free" anion in **12** with those in complexes **2**, **3**, and **4**, the metrical effects of metallocene–anion ion pairing can be assessed. As can be seen in Table 9 that the average B–C(aryl) distances (1.653-

(38) Hunter, W. E.; Hrncir, D. C.; Vann Bynum, R.; Pentila, R. A.; Atwood, J. L. *Organometallics* **1983**, *2*, 750–755.

(39) Jodan, R. F.; Bajyur, C. S.; Willett, R.; Scott, B. *J. Am. Chem. Soc.* **1986**, *108*, 7410–7411.

Table 10. Comparison of Cation/Anion Separation Parameters in 2, 3, and 4

complex	Zr···H_3C (bridging) (Å)	Zr···B (Å)	∠Zr···CH_3–B (deg)
2	2.549(3)	4.16	161.8(2)
4	2.625(5)	4.31	171.1(3)
3	2.640(7)	4.30	176.6(4)

Table 11. Close Nonbonded Cation–Anion Contacts (Å) in 2, 3, and 4

2[a]		3[a]		4[a]	
C12–C21	3.597 (3.6)[a]	C9–C35	3.377 (3.8)	F5–C7	3.124 (3.15)
C7–C33	3.874 (3.8)	C19–C23	3.43 (3.8)	F5–C22	3.391 (3.35)
C7–C28	3.929 (3.8)	F5–C9	3.453 (3.35)	F10–C4	3.126 (3.15)
F10–C6	3.469 (3.35)	F6–C21	3.34 (3.35)	F15–C17	3.087 (3.35)

[a] Data in parentheses are calculated van der Waals distances using van der Waals radii for CH_3, C(aryl), and F of 2.0, 1.8, and 1.35 Å, respectively.[42]

(3) Å in 2, 1.66(1) Å in 3, 1.652(5) Å in 4, and 1.665(3) Å in 12) and the CH_3–B–C (aryl) angles (108.1° in 2, 109.0° in 3, 108.6° in 4, and 108.8° in 12) do not differ significantly. On the other hand, the B–CH_3 distances in 2, 3, and 4 (1.663(5), 1.66-(1), and 1.699(7) Å, respectively) are slightly (but noticeably) stretched compared to that in 12 (1.638(5) Å), with the difference between 4 and 12 being greatest at 0.06(1) Å. This latter result suggests that the electrophilic zirconocene cation indeed effects some weakening of the B–CH_3 bond. The relatively large disparity in 4 vs 12 is especially interesting and will be discussed in detail later.

4. Cation/Anion Separations in 2, 3, and 4. On proceeding from complex 2 to 4 to 3, there is a steady increase in the Zr···H_3C-(bridge) distance. The Zr···B distances in 3 and 4 are also longer than that in 2 (Table 10). These data indicate that the cation and anion are better separated in 3 and 4 than in 2. In principle, this greater separation could be the result of (a) a weakening of the Coulombic interaction between cation and anion; (b) a weakening of the localized coordinative interaction between the bridging methyl group and the Lewis acidic Zr metal center; (c) an increase in steric repulsions between the cation ancillary ligands and the anion aryl groups, or a combination of all these effects. It will be seen that the structural data shed some light on this issue.

In regard to Cp substituents which may alter the Zr electron-deficiency/Lewis acidity, TMS Cp substituents are known to be more electron-withdrawing than methyl substituents.[40] Thus, the electron-deficiency at Zr in 4 is not expected to be less than that of 2 or 3. Therefore, the longer Zr···H_3C and Zr···B distances observed in 4 cannot be ascribed to weakening of the Zr···H_3C interaction due to lessened Zr coordinative/electronic unsaturation. Rather, an examination of the close cation–anion contacts (i.e., less than van der Waals distances) in 4 versus 2 and 3 (Table 11) strongly suggests that the observed long Zr···B distance in 4 is mostly likely due to cation–anion steric repulsions. Note the distances F5–C7 = 3.124, F10–C4 = 3.126, and F15–C17 = 3.087 Å, which can be compared to sums of the corresponding van der Waals radii[42] of 3.15, 3.15, and 3.35 Å, respectively. Indeed, the noticeably elongated B–CH_3 bond in this complex (Table 9) suggests that the Lewis acidity of the metal center in 4 is probably greater than that in 2 or 3. A more electron-deficient Zr center would compete more effectively with $B(C_6F_5)_3$ for the bridging methyl group. Since the distance between the two Lewis acidic centers (Zr···B) in the present complex is limited by the steric repulsions, the B–CH_3 bond is slightly elongated to maximize the coordinative/electrostatic interactions. The increase in Zr Lewis acidity together with the greater nonbonded repulsions also explains why 4 tends to undergo ligand redistribution to form neutral species (*vide supra*).

Table 12. Out of Plane Angles (deg) in Complexes 2, 3, and 4

complex	α[a]	β[a]	$\alpha+\beta$
2	52.8	39.3	92.1
3	52.9	35.5	88.4
4	58.3	39.3	97.6

[a] See definition in III text.

As for the longer Zr···CH_3 distance in 3 compared to 2, from the fairly close Cp′···C_6F_5 nonbonded contacts in 3 (Table 11) it is clear that steric repulsions again play a major role, although electronic contributions cannot be excluded. In principle, the electron-donating Cp methyl substituents may depress the Lewis acidity at the Zr center and thereby weaken the bridging methyl coordination to it.[40] However, even in 2 where the steric repulsions are not as significant due to the less sterically demanding Cp″ ligands (Table 9), the observed Zr···CH_3 (bridging) distance is still significantly longer than the Zr–CH_3(terminal) distance. Furthermore, the closest Zr···H contacts (Zr···H34B = 2.25(3), Zr···H34C = 2.23(3) Å; see Figure 1) are longer than the Zr···H distance observed between the zirconocene cation and the weakly coordinated carborane anion in $(EtMe_4C_5)_2ZrMe^+(\eta^1\text{-}H_{12}C_2B_9)^-$ (2.12 Å),[12j] in $Cp_2Zr(H)BH_3CH_3$ (2.00(3) and 2.04(4) Å)[41a] as well as the Zr···HCH_2CH_2 "agostic" interaction (2.16 Å) in cationic $(MeC_5H_4)_2Zr(CH_2CH_3)PMe_3^+BPh_4^-$.[41b] This indicates that even in the absence of strong steric repulsions, the cation and anion are still well-separated due to the low nucleophilicity of the $MeB(C_6F_5)_3^-$ methyl group.

5. Zr-CH_3(terminal) and Zr···CH_3(bridge) Out-of-Plane Angles. Drawing a line between Zr and the midpoint (C) of the two Cp centers of gravity (Cg) defines four angles (α, β, γ and θ), as shown schematically in III (viewed along the vector between the two Cp ring centroids, see Figures 1–3). The sum of the four angles in 2, 3, and 4 is 359.9°, 360°, and 359.9°, respectively. This means midpoint C, Zr, and the two methyl groups are essentially coplanar in all three complexes. Therefore, angles α and β define the out-of-plane angles of the two methyl groups with respect to the plane defined by Zr and the two ring Cg's. It has been shown before that in a series of L_2ZrX_2 complexes (L = Cp or Cp′; X = Me, CH_2TMS or CO) the X–Zr–X angle ranges from 86 to 98°, which corresponds to a α value of 43 to 49°.[43a] On the other hand, in the trivalent complex $(1,3\text{-}^tBu_2)_2ZrCl$, the angle α is zero.[23] For the present cationic zirconium complexes, it is of interest to inquire whether α contracts as the anion is translated away from the cation. As can be seen

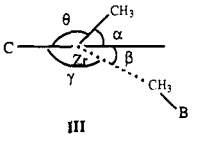

III

from Table 12, the experimental findings are somewhat surprising. Comparing 2 to 3, it can be seen that β decreases as the anion is moved away from the cation (presumably to minimize cation/anion nonbonded repulsions), while the α angle remains unchanged. On the other hand, in 4, which also has a larger cation–

(40) (a) Ryan, M. F.; Siedle, A. R.; Burk, M. J.; Richardson, D. E. *Organometallics* **1992**, *11*, 4231–4237. (b) Richardson, D. E.; Ryan, M. F.; Khan, N. I.; Maxwell, K. A. *J. Am. Chem. Soc.* **1992**, *114*, 10482–10485. (c) Gassman, P. G.; Winter, C. H. *Organometallics* **1991**, *10*, 1592–1598. (d) Gassman, P. G.; Deck, P. A. *Organometallics* **1992**, *11*, 959–960.

(41) (a) Kot, W. K.; Edelstein, N. M.; Zalkin, A. *Inorg. Chem.* **1987**, *26*, 1339–1341. (b) Jordan, R. F.; Bradley, P. K.; Baenziger, N. C.; LaPointe, R. E. *J. Am. Chem. Soc.* **1990**, *112*, 1289–1291.

(42) Ladd, M. F. *Structure and Bonding in Solid State Chemistry*; John Wiley & Sons: New York, 1979, p 253.

(43) (a) Schock, L. E.; Brock, C. P.; Marks, T. J. *Organometallics* **1987**, *6*, 232–241. (b) Recent theoretical work suggests that $\alpha \neq 0$ has electronic structural origins in such cationic metallocene complexes. See: ref 56 and Woo, T. K.; Fan, L.; Ziegler, T. *Organometallics* **1994**, *13*, 2252–2261.

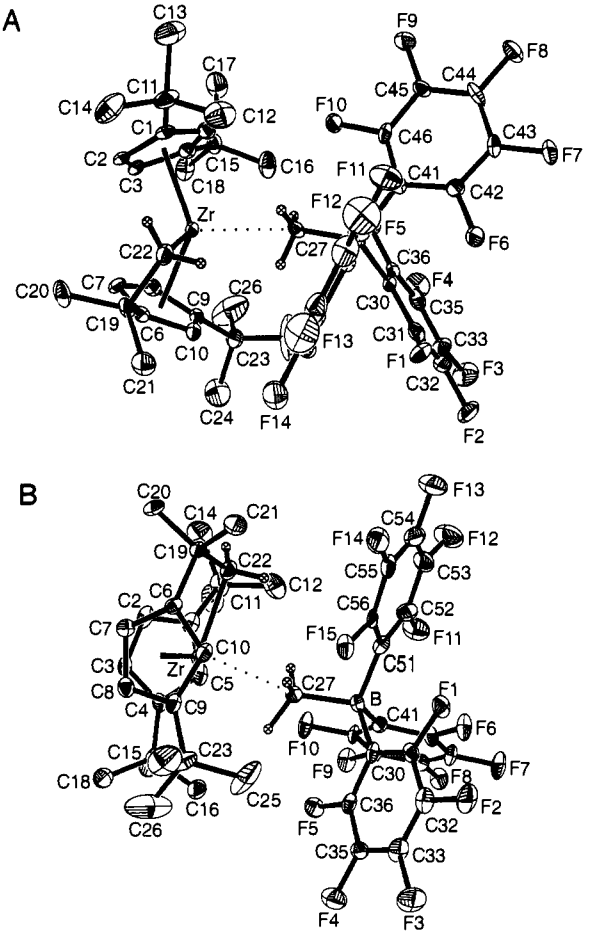

Figure 4. Perspective ORTEP drawings of the molecular structure of complex **6**. Thermal ellipsoids are drawn at the 50% probability level. (A) Viewed along the metalated ligand methyl carbon-Zr vector. (B) Viewed approximately along the ring Cg–ring Cg vector. The dotted lines are drawn as a guide to the eye.

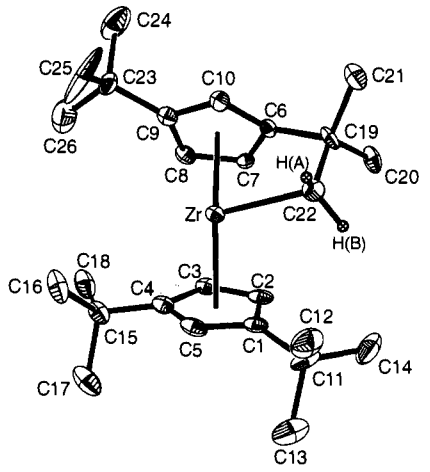

Figure 5. A close-up view of the cation in complex **6**.

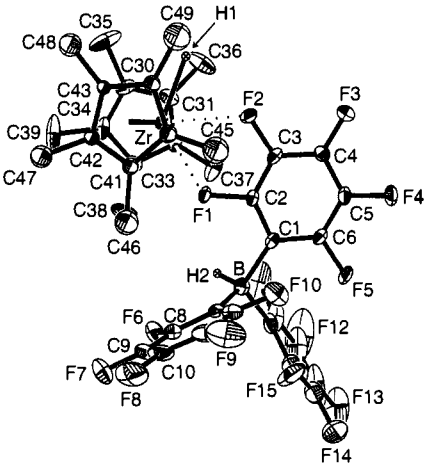

Figure 6. Perspective ORTEP drawing of cationic hydride complex **8**. Only one of the two possible orientations of the disordered Cp′ ring (C40–C44) is shown. Thermal ellipsoids are drawn at the 50% probability level. The dotted lines are drawn as a guide to the eye.

anion separation than **2**, the β angle is the same as in **2** while α increases (e.g., the terminal methyl group swings *away* from the aforementioned Cg–Zr–Cg plane). This increased α angle is probably a result of minimizing steric repulsion between the terminal Zr–CH_3 group with the TMS groups on the Cp-rings. This can be seen in Figure 3B. In summary, the structural results for complexes **3** and **4** evidence no systematic decrease of α as the anion is translated away from the cation.[43b]

B. Structure of Complex 6. The X-ray diffraction-derived molecular structure of **6** confirms the metallacyclic, η^6 configuration proposed on the basis of the NMR data (Figure 4). Again, the Zr cation weakly interacts with the anion through an unsymmetrical Zr···H_3C–B bridge. The Zr···CH_3 (bridging) distance of 2.624(1) Å is slightly shorter than that in **3** (2.640(7) Å) and is almost identical to that in **4** (2.625(5) Å). The three ^{t}Bu groups and the dimethylethyl group adapt a nearly eclipsed configuration (Figure 4B). This is quite different from the staggered geometry observed in complex **4** (Figure 3B).

A close-up view of the **6**-cation is shown in Figure 5. It can be seen that the top Cp ring is slightly tilted due to the formation of the η^6-Cp metallacyclic structure (the Zr to C6, C7, C8, C9, and C10 distances are 2.422(9), 2.40(1), 2.49(1), 2.61(1), and 2.48(1) Å, respectively). The top Cp ring also appears to be slightly closer to the Zr center than the bottom one (the Zr–C(ring) (av) distances are 2.48(1) and 2.51(1) Å, respectively). The Cg–Zr–Cg angle of 130.6° is 6° smaller than in **3** but very close to that in **2**, **4**, and **12**. The Zr–C(22) distance of 2.32(1) Å is only slightly longer than the terminal Zr–CH_3 bond in complexes **2**–**4** (*vide supra*) but close to the Zr–CH_2 bond distance in $Cp_2Zr(CH_2PPh_2)_2$ (2.284(8) and 2.340(9) Å).[44] The two hydrogen atoms on C22 have been refined isotropically. Their normal positions (∠Zr–C22–H22A = 115(5)°, ∠Zr–C22–H22B = 98(5)°) and long distance from the Zr atom (Zr–H22A = 2.89, Zr–H22B = 2.62 Å) rule out any unusual interactions (e.g., "agostic") with the metal.

Interestingly, despite the formation of the metallacyclic ring, σ-bonded C22 lies approximately in the plane defined by C27, Zr, and the midpoint of the two Cg's, a feature observed in the other $L_2ZrCH_3^+$ complexes. On the other hand, out-of-plane angles of C22 and C27 (α and β) are 71.4 and 20.6° (see **III**), respectively, indicating that C22 is pushed further away from the plane defined by Zr and the two Cg's, while C27 is closer to it. This apparently reflects a minimization of cation–anion steric repulsions. The B–C27 and B–C(aryl, av) distances of 1.66(1) and 1.65(1) Å, respectively, as well as the C27–B–C(aryl, av) angle of 109(1)° are unexceptional compared to those in complexes **2**, **3**, **4**, and **12**.

C. Structure of the Cationic Hydride $Cp'_2ZrH^+HB(C_6F_5)_3^-$ (8). The crystal structure of **8** is similar to the cationic zirconium methyl complexes discussed above in that it also consists of cation–anion pairs. However, there is a major difference that instead of a Zr···H–B bridge (as in $(EtMe_4C_5)_2ZrCH_3^+(\eta^1\text{-}H_{12}C_2B_9)^-$)[12j] to connect the cation and anion, as might be expected by analogy to the aforementioned Zr···H_3C–B bridges, the anion weakly coordinates to the cation through two Zr···F bridges (Figure 6).

(44) Shore, N. E.; Young, S. E.; Olmstead, M. M.; Hofmann, P. *Organometallics* **1983**, *2*, 1769–1780.

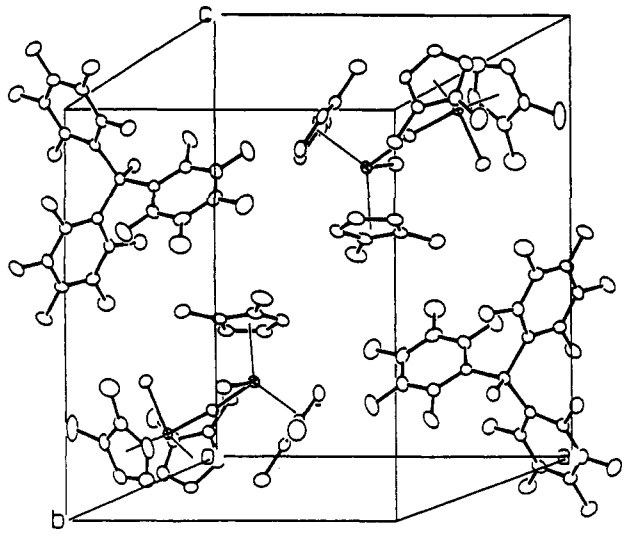

Figure 7. Packing diagram of a unit cell of complex **12**.

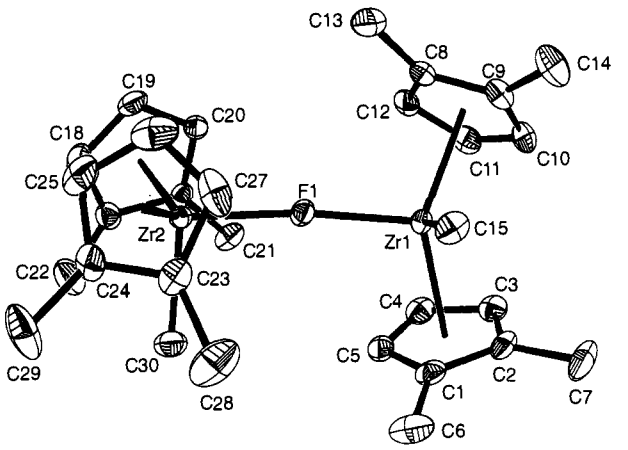

Figure 8. Perspective ORTEP drawing of the cation in complex **12**. Thermal ellipsoids are drawn at the 35% probability level. Protons are omitted for clarity.

The relatively long Zr···F distances (Zr–F1 = 2.416(3), Zr–F2 = 2.534(3) Å, Table 14) indicate that these interactions are fairly weak. They can be compared to Zr–F = 1.98(1) Å in Cp_2ZrF_2[45] and 2.108(2), 2.118(2) Å for the Zr–F–Zr fragment of **12** (*vide infra*). There is a small but noticeable enlongation of the C_2–F_1 bond (1.396(5) vs 1.354(4) Å for the average C–F distance in the anion), while the effect in the C_3–F_2 bond (1.379(6) Å) is less evident. Considering that the Zr–F_1(2.416(3) Å) distance is also shorter than Zr–F_2 (2.534(31) Å), it seems clear that Zr···F_1 interaction is in fact stronger than Zr···F_2. Interestingly, such an instantaneous coordination geometry is observed in a toluene solution at low temperatures (below –30 °C, by ^{19}F NMR). There are two factors which are likely to be responsible for the adoption of such a configuration. Most important is that steric constraints about the Zr center appear to preclude the close borane approach needed to form a relatively short Zr–H–B linkage. Furthermore, it seems likely that the hydridic character of the H–B functionality is diminished by the electron-withdrawing pentafluoroaryl substituents. This is supported by the finding that the present B–H distance of 1.06(6) Å appears to be shorter than the B–H (terminal) distance in the borate complex $Cp_2Zr(H)BH_3CH_3$ (1.32(10) Å).[41a]

D. Structure of $[Cp_2''(CH_3)Zr(\mu\text{-}F)Zr(CH_3)Cp_2'']^+[CH_3B(C_6F_5)_3]^-$ (12). The crystal structure of **12** consists of discrete $[Cp''_2(CH_3)Zr\text{–}F\text{–}Zr(CH_3)Cp''_2]^+$ cations and $CH_3B(C_6F_5)_3^-$ anions, instead of closely associated cation/anion pairs as in the case of **2** and **3** (Figure 7, Table 15). A close-up view of the cation is shown in Figure 8. The fluoride-bridged cation has a nearly linear Zr–F–Zr configuration (Zr1–F–Zr2 = 173.3(1)°). The two Cp''_2ZrCH_3 fragments are crystallographically nearly identical (e.g., Zr1–F1 = 2.108(2) Å, Zr2–F1 = 2.118(2) Å, Zr1–C15 = 2.219(4) Å, Zr2–C30 = 2.224(4) Å, Zr1–C(ring)(av) = 2.509(3) Å, Zr2-C(ring)(av) = 2.505(3) Å). The present Zr–C(ring)(av) distance is close to, while the Zr–CH_3 distance is slightly shorter than, the corresponding distances in **2** (*vide supra*). The present Zr–(μ-F) distance is also longer, as expected, than the Zr–F distance in Cp_2ZrF_2 (1.98(1)Å).[45] Relevant structural features of the anion have been discussed in conjunction with other complexes in the previous sections.

IV. Metallocene Ion Pair Solution Structural Dynamics. Although the preceding analyses provide a detailed picture of the *static*, metrical aspects of $L_2ZrR^+CH_3B(C_6F_5)_3^-$ ion pairing, they reveal little about the dynamics. Elucidating the pathways and energetics by which such highly reactive ion pairs can be separated/deformed/reorganized, especially in the present low-dielectric, noncoordinating media, is crucial to ultimately understanding polymerization activity, chain transfer processes, and stereoregulation. The present metallocene ion pairs have several unique structural features which allow probing of these questions by dynamic NMR spectroscopy.

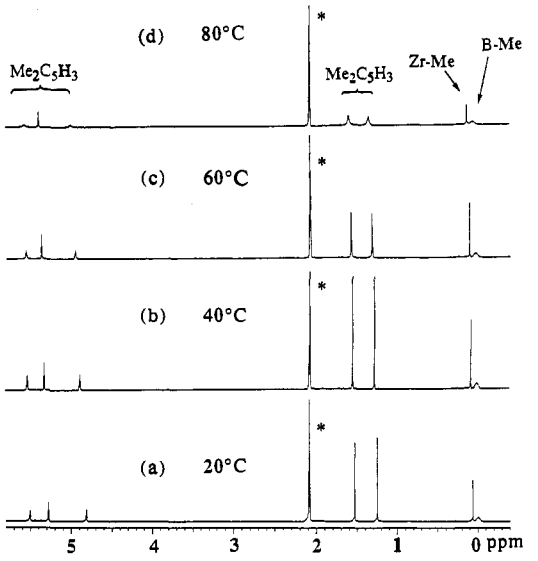

Figure 9. Variable temperature ^{1}H NMR spectra of complex **2** as a solution in toluene-d_8. The asterisk denotes a solvent signal.

A. Cation–Anion Dissociation/Reorganization and Zr–Me/B–Me Exchange Processes in 2. Shown in Figure 9 are a series of variable-temperature ^{1}H NMR spectra for complex **2** in toluene-d_8. There are several features which yield solution structural information about the ion pairing. Firstly, the observation of two types of Cp ring methyl signals (δ 1.51 and 1.20 ppm) and three types of Cp ring proton signals (δ 5.49 (t), 5.23 (t), 4.78 (t) ppm, equal intensity) suggests relatively immobile ion pairing for **2**, with symmetry similar to what is observed in the solid state (**IV**). In such a configuration, the two methyl groups on each Cp ring and the two ring protons adjacent to the two methyls are formally diastereotopic and should give rise to

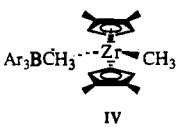

IV

magnetically distinct ^{1}H NMR signals. Secondly, it can be seen that as temperature is increased, all the resonances except that at δ 5.23 ppm undergo broadening, indicating the onset of exchange process(es). These features are reversible upon lowering the

(45) Bush, M. A.; Sim, G. A. *J. Chem. Soc. (A)* **1971**, 2225–2229.

Scheme 2. Solution Dynamic Processes for Complex **2**

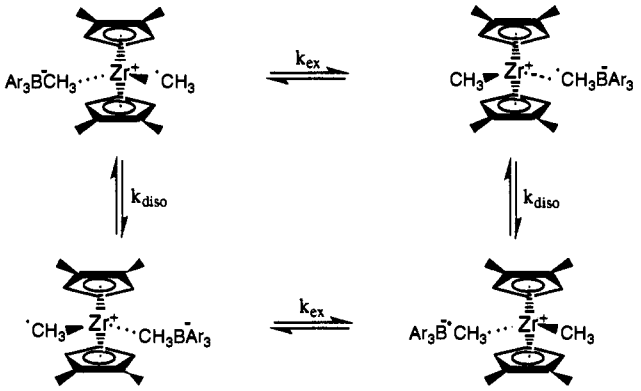

temperature. Furthermore, the broadening of the signals corresponding to the Cp″ ligands is greater (~6 times greater for a given temperature than the Zr–Me/B–Me broadening). The above observations are consistent with the coexistence of two types of exchange processes: (a) ion-pair dissociation/reorganization which causes the broadening of the Cp″ signals only and (b) Zr–Me/B–Me exchange which causes the broadening of both Cp″ and Zr–Me/B–Me signals, simultaneously (Scheme 2). These spectroscopic changes are invariant over a 10-fold concentration range.

Assuming that at room temperature both exchange processes are sufficiently slow as not to contribute to the NMR line broadening (this is a reasonable assumption because as there is essentially no detectable line broadening between −20 °C to 40 °C), rate constants for the Zr–Me/B–Me exchange (k_{ex}) and for the two types of ring methyl exchange ($k_o = k_{ex} + k_{diso}$; where k_{ex} and k_{diso} are the Zr–Me/–Me exchange and the ion pair dissociation/reorganization rate constants, respectively) can be derived from the line width changes of the Zr–Me and ring methyl resonances, respectively, using the standard modified Bloch two-site exchange formalism (eq 10). Here k is the rate constant in s^{-1}; $\Delta W = W_2 - W_1$, where W_2 is linewidth at half-height of

$$k = \pi \Delta W \tag{10}$$

the exchange broadened peak, and W_1 is the line width in the absence of exchange.[46] The corresponding free energies of activation can also be derived using eq 11.[46] Kinetic results are summarized in Table 16. The tenfold concentration independence of the line shape changes argues that

$$\Delta G^{\ddagger} = -RT[\ln(k/T) + \ln(h/k)] \tag{11}$$

both of the exchange processes are unimolecular. These results are consistent with an essentially concerted transition state such as **V** for the Zr–Me/B–Me exchange process and a simple intramolecular dissociation/reassociation process for the ion pair reorganization process (k_{diso}).[47] Thermal decomposition precludes accurate NMR experiments with **2** at higher temperatures.

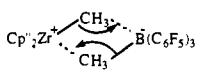

V

B. Cation–Anion Dissociation/Reorganization and Zr–Me/B–Me Exchange Processes in 4. Complex **4** has disymmetric structure similar to **2** and therefore solution structural dynamic properties can similarly be probed. Indeed, variable-temperature ^{1}H NMR properties are qualitatively similar to those of **2**. Using the similar analysis procedures, the ion-pair dissociation/reorganization and Zr–Me/B–Me exchange rate constants are found to be 358 s^{-1} (k_{diso}) and 5.0 s^{-1} (k_{ex}), respectively, at 35 °C (the coalescence temperature of the two Cp-Me's) (Table 16). These correspond to $\Delta G^{\ddagger}$ values of 14.4 and 18.0 kcal/mol, respectively. Thus, the barrier for the ion-pair dissociation/reorganization process in **4** is substantially lower than that of **2**. This can be attributed to the much greater steric hindrance of the ancillary ligands in **4**, as can clearly be seen from the crystal structure (*vide infra*). This should weaken the cation/anion attraction.

C. Comparison of Zr–Me/B–Me Exchange Kinetics in Complexes 1–4. The Zr–Me/B–Me methyl exchange rates in solution for complexes **1** and **3** can similarly be obtained from ^{1}H NMR line broadening of the Zr–Me resonances using the procedure described above. The results are summarized in Table 16. It can be seen that despite the dramatic differences observed in ion-pair dissociation/reorganization rates between **2** and **4**, the Zr–Me/B–Me exchange rates for complexes **1–4** are rather

Table 13. Selected Bond Distances (Å) and Angles (deg) for $(1,3\text{-}^tBu_2C_5H_3)(1,3\text{-}^tBuC_5H_3CMe_2CH_2)Zr^+CH_3B(C_6F_5)_3^-$ (**6**)

	Bond Distances		
Zr–C1	2.58(1)	Zr–C2	2.484(9)
Zr–C3	2.450(9)	Zr–C4	2.509(9)
Zr–C5	2.51(1)	Zr–C6	2.422(9)
Zr–C7	2.40(1)	Zr–C8	2.49(1)
Zr–C9	2.61(1)	Zr–C10	2.48(1)
Zr–C22	2.32(1)	Zr–C27	2.62(1)
C22–H22A	1.01(8)	C22–H22B	0.92(8)
C27–B	1.66(1)	C27–H27A	0.83(8)
C27–H27B	0.92(8)	C27–H27C	1.12(8)
C30–B	1.66(1)	C41–B	1.65(1)
C51–B	1.64(1)		
	Angles		
C22–Zr–C27	92.0(4)	Zr–C22–C19	103.5(7)
Zr–C22–H22A	115(5)	Zr–C22–H22B	98(5)
Zr–C27–B	165.0(7)	C22–C19–C6	97.7(7)
Zr–C27–H27A	71(6)	Zr–C27–H27B	67(5)
Zr–C27–H27C	76(4)	H27A–C27–H27B	104(8)
H27A–C27–H27C	117(7)	H27B–C27–H27C	110(6)
C27–B–C30	108.5(8)	C27–B–C41	114.6(8)
C27–B–C51	103.9(8)	C30–B–C41	103.3(8)
C30–B–C51	114.6(8)	C41–B–C51	112.1(8)

Table 14. Selected Bond Distances (Å) and Angles (deg) for $(C_5Me_5)_2ZrH^+HB(C_6F_5)_3^-$ (**8**)

	Bond Distances		
Zr–F1	2.416(3)	Zr–F2	2.534(3)
Zr–C30	2.508(5)	Zr–C40	2.46(1)
Zr–C31	2.513(5)	Zr–C41	2.47(1)
Zr–C32	2.494(5)	Zr–C42	2.520(9)
Zr–C33	2.479(5)	Zr–C43	2.499(8)
Zr–C34	2.510(5)	Zr–C44	2.493(9)
Zr–H1	2.00(5)	B–C1	1.638(8)
B–C7	1.621(8)	B–C13	1.639(8)
B–H2	1.06(6)	F1–C2	1.396(5)
F2–C3	1.379(6)	F3–C4	1.335(6)
F4–C5	1.344(6)	F5–C6	1.352(6)
F6–C8	1.362(8)	F7–C9	1.339(8)
F8–C10	1.357(8)	F9–C11	1.348(8)
F10–C12	1.339(7)	F11–C14	1.35(1)
F12–C15	1.35(1)	F13–C16	1.34(1)
F14–C17	1.39(1)	F15–C18	1.328(9)
	Angles		
H2–B–C1	104(3)	H2–B–C7	109(3)
H2–B–C13	105(3)	C1–B–C7	112.9(4)
C1–B–C13	111.9(4)		

(46) (a) Sandstrom, J. *Dynamic NMR Spectroscopy*; Academic Press: New York, 1982; pp 77–92. (b) Kaplan, J. I.; Fraenkel, G. *NMR of Chemically Exchanging Systems*; Academic Press: New York, 1980, pp 71–128.

(47) (a) These data do not, of course, rule out the possibility that the exchange processes are dissociative (S_N-1-like) in character and that rapid exchange with free $B(C_6F_5)_3$ or $MeB(C_6F_5)_3^-$ might ensue subsequent to unimolecular dissociation.[47b] These issues will be discussed in detail elsewhere.[47c] (b) Deck, P. A.; Marks, T. J. *Abstracts*, 207th Meeting of the American Chemical Society, San Diego, CA, March 13–17, 1994, INOR45. (c) Deck, P. A.; Marks, T. J., manuscript in preparation.

Table 15. Selected Bond Distances (Å) and Angles (deg) for $[(1,3\text{-}Me_2C_5H_3)_2ZrCH_3]_2(\mu\text{-}F)^+CH_3B(C_6F_5)_3^-$ (12)

	Bond Distances		
Zr1–F1	2.108(2)	Zr2–F1	2.118(2)
Zr1–C15	2.219(4)	Zr2–C30	2.224(4)
Zr1–C1	2.583(4)	Zr1–C2	2.565(4)
Zr1–C3	2.476(3)	Zr1–C4	2.429(4)
Zr1–C5	2.482(4)	Zr1–C8	2.549(4)
Zr1–C9	2.565(4)	Zr1–C10	2.478(4)
Zr1–C11	2.467(4)	Zr1–C12	2.493(4)
Zr2–C16	2.541(3)	Zr2–C17	2.565(4)
Zr2–C18	2.480(4)	Zr2–C19	2.454(4)
Zr2–C20	2.490(4)	Zr2–C23	2.598(4)
Zr2–C24	2.558(4)	Zr2–C25	2.455(4)
Zr2–C26	2.417(4)	Zr2–C27	2.489(4)
C31–B	1.656(6)	C42–B	1.669(5)
C43–B	1.671(5)	B–C50	1.638(5)
	Angles		
F1–Zr1–C15	91.8(1)	F1–Zr2–C30	95.8(1)
Zr1–F1–Zr2	173.3(1)	C31–B–C42	112.6(3)
C31–B–C43	110.3(3)	C31–B–C50	106.2(3)
C42–B–C43	107.7(3)	C42–B–C50	108.8(3)
C43–B–C50	111.3(3)		

Table 16. Rate and Free Energy of Activation for the Solution Dynamic Processes of Complexes 1–4 in Toluene-d_8

		ion-pair dissociation		Zr–Me/B–Me exchange	
complex	temp (°C)	k (s^{-1})	$\Delta G^{\ddagger}_{diso}$ (kcal/mol)	k (s^{-1})	$\Delta G^{\ddagger}_{ex}$ (kcal/mol)
1	80			18.2(1)	18.7(2)
2	80	29.85(1)	18.3(2)	4.41(1)	19.7(2)
3	80			3.80(1)	19.8(2)
4	35	358.0(1)	14.4(2)	5.02(1)	18.0(2)

similar. The Zr-Me/B-Me exchange rate is much *less sensitive* to ancillary ligation/coordination environment around the metal center than is the ion-pair dissociation/reassociation process. Nevertheless, $\Delta G^{\ddagger}$ for **4** is significantly smaller than for other complexes. This agrees with the foregoing observation that **4** has a slightly stretched B–CH_3 bond in the solid state compared to the other complexes, a result associable with greater electron-deficiency at the Zr metal center. Interestingly, the activation barriers obtained here appear to be higher than those reported for Zr–Me/Al–Me exchange between Cp_2ZrMe_2 and MAO ($\Delta G^{\ddagger}$ = 13.9 kcal/mol at 25 °C), suggesting that the B–Me bond is kinetically less labile than the respective Al–Me bond (assuming similar ion pair structures).[48]

V. Catalytic Polymerization of Olefins by Borane-Derived Cationic Zirconocenes. A. Polymerization of Ethylene by Complexes 1–4, 7, and 8. The crystallographic and solution dynamic NMR studies of the $L_2ZrCH_3^+CH_3B(C_6F_5)_3^-$ complexes discussed above reveal that the $CH_3B(C_6F_5)_3^-$ anion is relatively weakly coordinated and that the cationic Zr–CH_3/Zr–H center has significant 14 electron character. This suggests that these cationic zirconium complexes should be active catalysts for the polymerization of olefins. Experimental results confirm this. When gaseous ethylene (1 atm of pressure) is admitted to rapidly stirred toluene (or benzene) solutions of complexes **1–4, 7, 8**, and under rigorously anhydrous, anaerobic conditions, solid polyethylene precipitates within seconds. The turnover frequencies (Table 17), as determined by quenching the polymerization reactions after a measured time interval and weighing the quantity of the polymer produced, suggest that the activities of these complexes are much higher than those of simple cationic group 4 metal complexes having BPh_4^-[11b] or bulky carborane ($H_{12}C_2B_9^-$)[12j] charge-compensating anions and approach the activity of the zirconocene/methylalumoxane catalyst systems

(48) Siedle, A. R.; Newmark, R. A.; Lamanna, W. M.; Schroepfer, J. N. *Polyhedron* **1990**, *9*, 301–308.

Table 17. Ethylene Polymerization Activities and Polymer Properties[a]

catalyst	concn (mM)	reaction time (s)	PE (g)	activity g/mol h atm (×10⁶)	M_w (×10³)[b]	M_n (×10³)[b]	M_w/M_n
1	0.32	40	0.65	4.5	124.0	61.2	2.0
2	0.22	66	1.1	6.8	521.4	367.4	1.4
3	0.22	56	0.75	5.4	136.0	53.6	2.5
4	0.22	62	0.58	3.8	255.0	126.0	2.0
8	0.21	78	0.61	3.2	434.3	154.4	2.8

[a] Carried out at 25 °C, 1 atm of ethylene, 40 mL of toluene. [b] GPC in 2,4,6-trichlorobenzene vs polystyrene.

under similar conditions.[2,3] The polyethylenes produced by the present catalysts are highly linear as shown by ^{13}C NMR spectroscopy and have relatively high molecular weights as indicated by GPC (Table 17).[49]

B. Polymerization of Propylene. Competing β-H Shift and β-Alkyl Shift Processes as Chain Transfer Mechanisms. Complexes **1**, **2**, **3**, and **8** are also active for the polymerization of propylene under 1–8 atm of propylene pressure (see Experimental Section for details) to form colorless, viscous oils (Table 18). ^1H and ^{13}C NMR spectroscopic analysis of the resulting polypropylenes reveals that they are typically atactic. The molecular weights are relatively low, indicating high termination/insertion ratios.

Interestingly, although polypropylene derived from **1** and **2** contains only vinylidene/*n*-propyl end groups (as assessed by ^1H NMR),[49] which is consistent with a "normal" 1–2 monomer insertion/β-H elimination mechanism (Scheme 3, pathway **A**), polypropylene from **3** and **8** contains *both* vinyl/isopropyl and vinylidene/*n*-propyl end groups, with the former dominating (ca. 6:1 ratio by ^1H NMR). The formation of vinyl/isopropyl end groups is particularly interesting. In principle, they can most reasonably arise from at least two different processes: β-CH_3 elimination and allylic C–H activation, both of which have ample literature precedent in analogous, isoelectronic organoscandium and organolanthanide chemistry (Scheme 3, pathways B, C).[13–15] A 2–1 insertion of the last inserted monomer coupled with a β-H elimination should generate vinyl/*n*-propyl type end groups (Scheme 3, pathway D) and should be less probable on steric grounds in the present case. In order to probe the exact mechanism of the chain termination process, the oligomerization of [3-^{13}C] propylene by the catalyst $Cp'_2ZrH^+HB(C_6F_5)_3^-$ (**8**) was studied in toluene-d_8 (see Experimental Section for details). This catalyst was chosen since initiation is expected to be more rapid than for the Zr–CH_3^+ analogue **3**. As can be seen from Scheme 3, these different chain termination mechanisms will give rise to distinctively different ^{13}C labeling patterns in the products. Shown in Figure 10 is the 100 MHz $^{13}C\{^1H\}$ NMR spectrum of the propylene oligomers. It can be seen that for the end groups,[50] ^{13}C enrichment occurs exclusively at the isopropyl (δ 22.5 and 23.5 ppm) and, to a lesser extent, *n*-propyl (δ 14.5 ppm) methyl positions. This reveals that the β-CH_3 elimination pathway is responsible for the formation of the vinyl/isopropyl end groups (pathway B in Scheme 3) and is the predominant chain transfer pathway. The lack of ^{13}C enrichment at the δ 42–44 and 116 ppm positions also confirms that 2–1 insertion/β-H elimination is not important under the present conditions. Furthermore, allylic C–H activation processes[13–15] can be rigorously ruled out as a significant chain termination pathway. These results are in agreement of what has recently been inferred by two other groups in related catalytic systems using different analytical approaches

(49) (a) *Encyclopedia of Polymer Science*; Wiley: New York, 1987, Vol 10, pp 298–299. (b) Bovey, F. A. *Chain Structure and Confirmation of Macromolecules*; Academic Press: New York, 1982, pp 78–91.

(50) Tsutsui, T.; Mizuno, A.; Kashiwa, N. *Polymer* **1989**, *30*, 428–431.

Scheme 3. Propylene Polymerization and Chain Transfer Processes Potentially Mediated by Zirconocene Cations

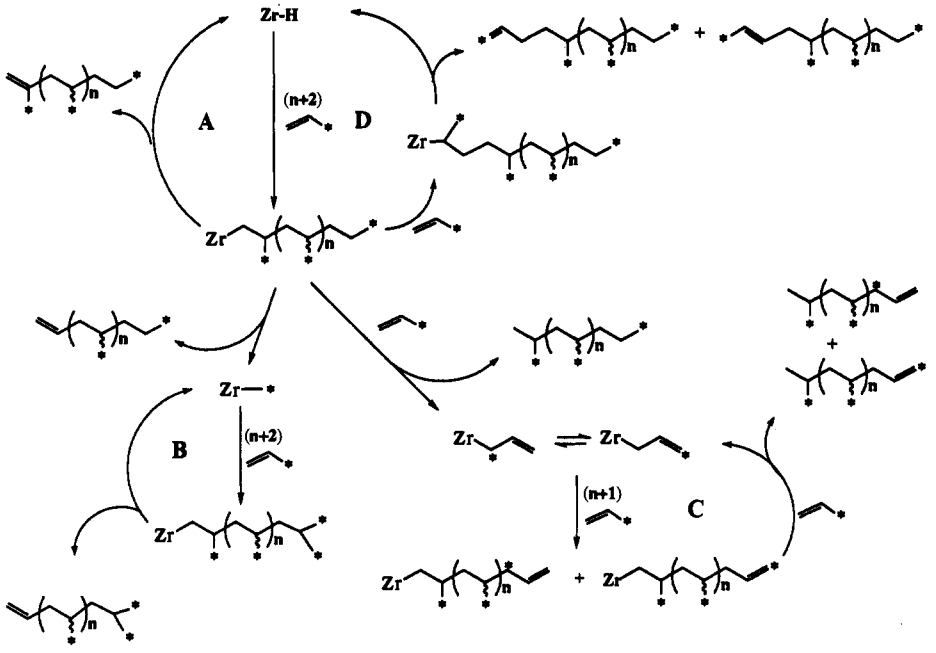

A = 1-2 Insertion, β-H Elimination
B = 1-2 Insertion, β-CH_3 Elimination
C = 1-2 Insertion, Allylic C-H Activation
D = 2-1 Insertion, β-H Elimination
* = ^{13}C Label

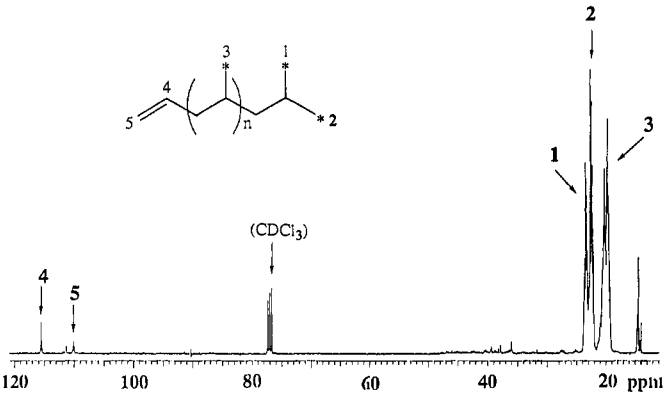

Figure 10. ^{13}C NMR spectrum of the oligomerization products derived from the reaction of $Cp'_2ZrH^+HB(C_6F_5)_3^-$ (**8**) with [3-^{13}C] propylene in $CDCl_3$. Peak assignments are according to ref 50. Peaks around 14.5 ppm are due to a small percentage of *n*-propyl end groups ($-CH_2CH_2{}^{13}CH_3$). See text for details.

and/or deuterium labeling.[51] However, in those studies, allylic C–H activation could not be rigorously excluded. Comparison of the present results with the literature results also reveals that the preference for β-CH_3 elimination processes by Cp'_2Zr^+R cation is an intrinsic property of the cation, which is not particularly sensitive to the anion (e.g., between $MeB(C_6F_5)_3^-$, $HB(C_6F_5)_3^-$, BPh_4^-, and MAO). The origin appears to be the cation-centered steric effects which orient the growing polymer chain in such a way that the configuration with the Zr^+ and β-CH_3 in a *syn*-periplanar relationship (presumably requisite for β-CH_3 elimination, **VI**) has lower ligand-polymer chain repulsions than the one with β-H and Zr^+ in a *syn*-periplanar relationship (requisite for β-H elimination, **VII**).[51]

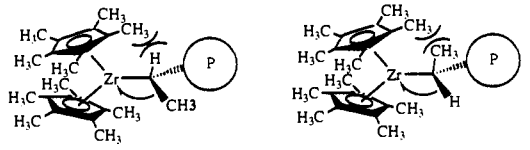

VI VII

C. Catalytic Dimerization of Propylene by Complex 9. Unlike complexes **1–3**, complex **9** does not mediate propylene polymerization to high molecular weight polymers (or even oligomers). Instead, it selectively *dimerizes* propylene to a mixture of 2-methyl-1-pentene and 2-methyl-2-pentene (identified by NMR and GC-MS), with a turnover frequency (N_t) of 0.25 s^{-1} at 0 °C under 1 atm of propylene pressure. The formation of 2-methyl-2-pentene is most likely through the in situ isomerization of 2-methyl-1-pentene; consistent with this hypothesis, a higher 2-methyl-1-pentene to 2-methyl-2-pentene ratio is observed by in situ ^1H NMR at early stages of the reaction. This product is likely formed via a simple insertion/β-H elimination mechanism (eq 12). It appears that the unique steric environment provided by the cyclopentadienyl ancillary ligation of **9** considerably alters the ratio of insertion to β-H elimination rates.

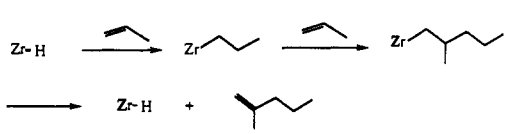

(12)

VI. Further Discussion. A. Active Center Formation and the Role(s) of the Lewis Acid Cocatalysts. The results of this study

(51) Chain transfer processes accompanying propylene polymerization have been studied by Teuben and co-workers in the less active $Cp'_2Zr(THT)^+BPh_4^-$ model system[51a] and by Resconi and co-workers in the compositionally more complex Cp'_2ZrMe_2/MAO system.[51b] Although their results unambiguously demonstrate that β-Me elimination is a major pathway for the formation of such endgroups, only the present results using ^{13}C-labeled monomer also rigorously rule out the possibility of C–H activation as a competing mechanism, in a structurally well-characterized and catalytically highly reactive system. (a) Eshuis, J. W.; Tan, Y. Y.; Teuben, J. H. *J. Mol. Catal.* **1990**, *62*, 277–287. (b) Resconi, L.; Piemontesi, F.; Franciscono, G.; Abis, L; Fiorani, T. *J. Am. Chem. Soc.* **1992**, *114*, 1025–1032.

Table 18. Propylene Polymerization Activities and Polymer Properties[a]

catalyst (mmol)	propylene (mL)	toluene (mL)	temp (°C)	reaction time (h)	yield of PP (g)	efficiency (g/mol h) (×10⁵)	M_w	M_n
1[b] (9.83)	6	2	20	0.50	3.0[c]	3.1	7000[e]	1700[e]
3[b] (6.64)	10	4	0	1.75	5.5[d]	4.7		1000[f]
8 (8.88)	14	4	0	2	5.5	3.2	3890[e]	2490[e]

[a] Carried out in a quartz Warden vessel. Propylene was measured as a liquid at −78 °C. [b] Monomer was completely consumed in these runs. Therefore the measured activities only represent the lower limit of the true values. [c] Pentad compositions: mmmm (0.06), mmmr (0.12), rmmr (0.07), mmrr (0.10), mmrm + rmrr (0.25), mrmr (0.15), rrrr (0.05), rrrm (0.12), mrrm (0.09). [d] Pentad compositions: mmmm (0.06), mmmr (0.07), rmmr (0.06), mmrr (0.09), mmrm + rmrr (0.18), mrmr (0.18), rrrr (0.05), rrrm (0.17), mrrm (0.11). [e] By GPC vs polystyrene. [f] By ^{1}H NMR.

argue that in $L_2ZrMe_2/B(C_6F_5)_3$-catalyzed olefin polymerization reactions the active centers are cationic L_2ZrMe^+ species. The principal role of the $B(C_6F_5)_3$ cocatalyst is to act as a Lewis acid which abstracts a methide (alkide) or hydride anion and by doing so creates and maintains the coordinative unsaturation and electron deficiency at the metal center necessary for substrate activation. *One obvious question which arises is that, of the many Lewis acids possible, why are only a very few such as $B(C_6F_5)_3$, MAO, AlR_nCl_{3-n}, $MgCl_2$, and DA actually capable of forming active olefin polymerization catalysts when combined with group 4 metallocenes.*

In comparison to simple Lewis acids, $B(C_6F_5)_3$ possesses *all of* the following properties: (a) high Lewis acidity, (b) low substituent nucleophilicity, and (c) high thermal and chemical stability. We hypothesize that these are the necessary requirements for a Lewis acid to be an effective metallocene polymerization cocatalyst. The requirement of high Lewis acidity is simply because if the cocatalyst is not more acidic (electrophilic) than the resulting cationic complex (e.g., L_2ZrMe^+), which is itself a very strong Lewis acid, then the equilibrium of eq 1 will lie far to the left. This requirement alone excludes many simple Lewis acids from being effective cocatalysts. However, high acidity alone cannot guarantee that a Lewis acid is an effective cocatalyst. For instance, although BX_3 reagents (X = F, Cl, Br, I) have comparable or even greater Lewis acidities than $B(C_6F_5)_3$,[17] they are not good candidates, because the halide atoms can either strongly coordinate to, or irreversibly transfer to, the group 4 cations. For the same reasons, PF_5 and SbF_5 are also not expected to be effective co-catalysts.[5a,11,52]

Although aluminum alkyl chlorides AlR_nCl_{3-n} form active ethylene polymerization catalysts when combined with titanocenes or zirconocenes, activities are far lower than the present zirconocene/$B(C_6F_5)_3$ systems. Furthermore, these catalysts are essentially inactive for the polymerization of less reactive α-olefins. This can be understood as a result of chloride coordination. For instance, in the $Cp_2TiCl_2/Al(CH_3)Cl_2$ system, although the existence of the ionic $Cp_2TiCH_3^+AlCl_4^-$ species has been proposed on the basis of chemical trapping studies, the only spectroscopically observable and isolable species is a chloride-bridged complex which itself is not an active catalyst (**VIII**, eq 13).[7]

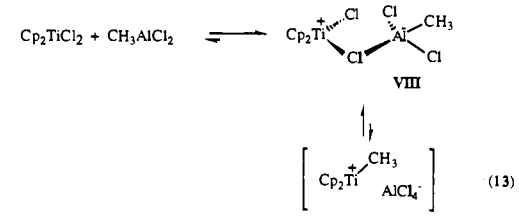

(13)

B. Solid State and Solution Structure of the Ion Pair. The present X-ray crystallographic studies unimbiguously demonstrate the "cation-like" character of these zirconocene complexes in the solid state (i.e., they are more accurately described by structure **IX** than **X**). As noted above, solution ^{1}H and ^{13}C NMR reveal

Table 19. Zr–$^{13}CH_3$ ^{13}C NMR Chemical Shifts for Molecular and Surface Cationic Zirconocene Species

complex	Zr–$^{13}CH_3$ (ppm)	ref
$Cp_2ZrCH_3^+CH_3B(C_6F_5)_3^-$	40.9,[a] 39.8[b]	this work, 55
$Cp_2Zr(CH_3)_2$/MAO	40.8[b]	10
$Cp_2ZrCH_3^+(THF)\ BPh_4^-$	38.9[b]	5b
$Cp_2Zr(CH_3)_2$/DA	36.0[b]	5b
$Cp_2Zr(CH_3)_2$	31.4[b]	5b
$Cp'_2ZrCH_3^+CH_3B(C_6F_5)_3^-$	50.4[a]	this work
$Cp'_2Zr(CH_3)_2$/MAO	47.7[b]	55
$Cp'_2Zr(CH_3)_2$	36.2[a]	21

[a] C_6D_6, 20 °C. [b] CPMAS solid state spectrum, 20 °C.

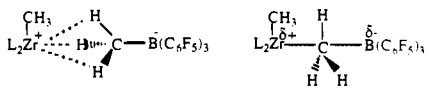

a Zr–CH_3 $^1J_{C-H}$ of 118 Hz (normal sp^3 carbon) for **3** which indicates that **IX** is also the preferred configuration in "noncoordinating" aromatic hydrocarbon solutions. In addition, the present cation solid state and solution phase Zr–$^{13}CH_3$ chemical shifts match well (Table 19) which further confirms the structural similarity of the cationic zirconium complexes in solution and in the solid state. Therefore, it is reasonable to suppose that the weak cation–anion coordinative interaction in all such complexes is mainly through the hydrogen atoms of the bridging methyl group. Direct metal–carbon interaction appears to be negligible. This situation is similar to the unsymmetrical, linear Lu–CH_3–Lu bridge in $(Cp'_2LuCH_3)_2$[13] but contrasts with the nearly symmetrical Zr–CH_3–Zr bridge in $[Cp_2Zr(OCCHCH_2C(CH_3)_3)]_2(\mu\text{-}CH_3)(\mu\text{-}Al(CH_3)_2)$.[53] In the latter, a Zr–CH_3 $^1J_{C-H}$ of 136.2 Hz is characteristic of sp^2 hybridization at the bridging CH_3 group. In regard to the transition state for methide abstraction, two extreme possibilities can be envisioned (**XI** or **XII**). Although there is no direct evidence to argue for one versus the other, steric considerations suggest **XI** is of lower energy.

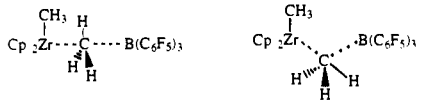

Another interesting structural result of this study is that, despite the electron-deficiency and coordinative unsaturation in the Zr center, the X-ray crystallographic studies give no evidence of α-"agostic" type interactions. This is true even in the case of **6** where the metallacyclic structure would appear to favor such an interaction (*vide supra*). Such α-"agostic" interactions have been

(52) (a) Bochmann, M.; Wilson, L. M. *J. Chem. Soc., Chem. Commun.* **1986**, 1610–1611. (b) Jordan, R. F.; Dasher, W. E.; Echols, S. F. *J. Am. Chem. Soc.* **1986**, *108*, 1718–1719.

(53) Waymouth, R. M.; Santasiero, B. D.; Coots, R. J.; Brunikowski, M. J.; Grubbs, R. H. *J. Am. Chem. Soc.* **1986**, *108*, 1427–1441.

the subject of considerable discussion concerning a role in influencing the rate and stereoregulation of the olefin insertion process.[43b,54,56]

3. Implications for MAO- and Surface-Based Catalysts. Methylalumoxane (MAO) and Lewis acidic surfaces (e.g., DA) are effective in activating group 4 metal complexes to form cationic metallocene polymerization catalysts. MAO has attracted considerable attention because of the extremely high catalytic activity associated with it. However, the role MAO plays has also been controversial,[1-3] mainly because of our extremely poor understanding of the structure. The requirement of large excesses of MAO to reach high activities makes it even more challenging to study this system in detail. Nevertheless, from the many similarities of the catalysts based on MAO and on $B(C_6F_5)_3$, it appears that the most important role of the cocatalysts in these different systems is, in fact, the same. Indeed, solid state ^{13}C NMR spectroscopic data for both MAO- and DA-based catalysts suggest the formation of electron-deficient cationic species which are similar to those generated with $B(C_6F_5)_3$ (Table 19).[9,10,55]

Conclusions

We have isolated and systematically studied the structural and chemical properties of a series of electron-deficient cationic zirconocene alkyl and hydrido complexes with high olefin polymerization activities. The single crystal X-ray diffraction-derived solid state and ^1H NMR-derived solution structures of these complexes correlate well with each other and afford considerable insight into the nature of these species. Such information is furthermore invaluable for calibrating theoretical studies.[56] More importantly, however, through the use of the novel organoborane $B(C_6F_5)_3$, we have, for the first time, unambiguously demonstrated the role of the key metallocene–cocatalyst interaction that has been proposed for MAO, alkyl aluminum halides, and dehydroxlated alumina.

Acknowledgment. This research was supported by the U. S. Department of Energy (Grant DE-FG02-86ER13511). X.Y. thanks Akzo Chemicals for a postdoctoral fellowship. We thank Dr. P.A. Deck for helpful discussions and Dr. D. A. Kershner of Akzo Research Laboratories for GPC analyses.

Note Added in Proof. After this paper was accepted for publication, the molecular structure of complex **4** was also reported by another group: Bochmann, M.; Lancaster, S. J.; Hursthouse, M. B.; Malik, K. M. A. *Organometallics* **1994**, *13*, 2235–2243. The results (298 K data collection) are in agreement with the present results.

Supplementary Material Available: X-ray experimental details including tables of positional and anisotropic displacement parameters and tables of bond lengths and angles (236 pages); listing of observed and calculated structure factor amplitudes (192 pages). This material is contained in many libraries on microfiche, immediately follows this article in the microfilm version of the journal, and can be ordered from the ACS; see any current masthead page for ordering information.

(54) (a) Brookhart, M.; Green, M. L. H. *J. Organomet. Chem.* **1983**, *250*, 395–408. (b) Clawson, L.; Soto, J.; Buchwald, S. L.; Steigerwald, M. L.; Grubbs, R. H. *J. Am. Chem. Soc.* **1985**, *107*, 3377–3378. (c) Cotter, W. D.; Bercaw, J. E. *J. Organomet. Chem.* **1991**, *417*, C1–C6. (d) Krauledat, H.; Brintzinger, H. H. *Angew. Chem. Int. Ed. Engl.* **1990**, *29*, 1412–1413. (e) Prosenc, M. H.; Janiak, C.; Brintzinger, H. H. *Organometallics* **1992**, *11*, 4036–4041. (f) Alelyunas, Y. W.; Baenziger, N. C.; Bradley, P. K.; Jordan, R. F. *Organometallics* **1994**, *13*, 148–156 and references therein.

(55) Sishta, C.; Marks, T. J., unpublished results.

(56) For recent theoretical work, see: (a) Bierwagen, E. P.; Bercaw, J. E.; Goddard, III, W. A., *J. Am. Chem. Soc.* **1994**, *116*, 1481–1489. (b) Woo, T.; Fan, L.; Ziegler, T. *Organometallics* **1994**, *13*, 432–433, and references therein. (c) Hart, J. R.; Rappé, A. K. *J. Am. Chem. Soc.* **1993**, *115*, 6159–6164, and references therein. (d) Gleiter, R.; Hyla-Kryspin, I.; Niu, S.; Erkert, G. *Organometallics* **1993**, *12*, 3828–3836. (e) Kawamura-Kuribayashi, H.; Koga, N.; Morokuma, K. *J. Am. Chem. Soc.*, **1992**, *114*, 8687–8694, and references therein.